Separation and Properties of La_2O_3 in Molten LiF-NaF-KF Salt

Qiufeng Yang

Thesis submitted to the faculty of the Virginia Polytechnic Institute and State University

In partial fulfillment of the requirements for the degree of

Master of Science

In

Nuclear Engineering

Jinsuo Zhang, Chair

Alireza Haghighat

Mark A. Pierson

December 7, 2018

Blacksburg, VA

Keywords: solubility, lanthanum oxyfluoride, electrochemical separation, graphite sacrificial anode electrode, first principle molecular dynamics simulation

Separation and Properties of La_2O_3 in Molten LiF-NaF-KF Salt

Qiufeng Yang

Abstract

Studies on nuclear technology have been ongoing since nuclear power became uniquely important to meet climate change goals while phasing out fossil fuels. Research on the fluoride salt cooled high temperature reactor (FHR), which is funded by the United States Department of Energy (DOE), has developed smoothly with the ultimate goal of a 2030 deployment. One challenge presented by FHR is that the primary coolant salt can acquire contamination from fuel failure and moisture leaking into the system. If contamination happens, it will result in a low concentration of fission products, fuel, transuranic materials and oxide impurities in the coolant. These impurities will then affect the properties of the molten salt in the long term and need to be removed without introducing new impurities. Most of the research conducted recently has focused on impurity separation in chloride molten salts. More research urgently needs to be conducted to study the impurity separation method for the fluoride molten salts.

In this study, the La_2O_3-LiF-NaF-KF (La_2O_3-FLiNaK) system is used to demonstrate impurity separation in molten fluoride salt. Since lanthanum oxide needs to be dissolved in the fluoride molten salt and studies in this field are still not complete, the solubility of lanthanum oxide in FLiNaK have been measured at different temperatures to obtain the temperature-dependent solubility and understand the corresponding dissolution mechanisms first. In the solubility related experiments, Inductively Coupled Plasma Mass Spectrometry (ICP-MS) is utilized to analyze the concentration of lanthanum ions in the molten FLiNaK salt, while X-ray powder diffraction (XRD) was applied to determine the phase patterns of molten salt. Second,

electrochemical experiments with tungsten and graphite as working electrodes were conducted individually to demonstrate the separation of the dissolved oxide from the salt. When the tungsten working electrode was applied, the lanthanum ions were reduced to lanthanum metal at the tungsten cathode, while the fluorine ions reacted with the tungsten anode to form tungsten fluoride. In the experiments, the production of tungsten fluoride could lead to increasing current in the cell, even overload. Moreover, theoretically, tungsten fluoride WF4 is soluble in the fluoride salt thus introducing new impurities. All these issues make tungsten not the best choice when applied to the separation of oxygen ions. Therefore, another common working electrode graphite is used. It not only has all the advantages of tungsten, but also has good performance on separation of oxygen ions. When the graphite electrode was applied, the lanthanum ions were separated in the form of lanthanum carbide (LaC_2), while the oxygen ions can be removed in the form of carbon dioxide (CO_2) or carbon monoxide (CO). In addition, only graphite was consumed during the whole separation process, which is why the graphite anode electrode is called the “sacrificial electrode”. Third, First Principle Molecular Dynamics (FPMD) simulations with Vienne Ab initio Simulation Package (VASP) was conducted to study the properties of the fluoride molten salt. In this study, the structure information and enthalpy of formation were obtained. Generally, the simulation process can be divided into four steps: (1) the simulation systems are prepared by packing ions randomly via Packmol package in the simulation cell; (2) an equilibrium calculation is performed to pre-equilibrate the systems; (3) FPMD simulations in an NVT ensemble are implemented in VASP; (4) based on the FPMD simulations results, the first peak radius and the first-shell coordination number were evaluated with partial radial distribution function (PRDF) analysis to determine the statistics of molten salt structure information, while the transport properties, e.g., the self-diffusion coefficient was calculated

according to the function of mean square displacement (MSD) of time generated by the Einstein-Smoluchowshi equation. The viscosity and ionic conductivity were obtained by combining the self-distribution coefficient with the Einstein-Stokes formula and Nernst-Einstein equation.

Separation and Properties of La_2O_3 in Molten LiF-NaF-KF Salt

Qiufeng Yang

General Audience Abstract

With the fast development of modern society and economy, more and more energy is urgently needed to meet the growth of industry. Since the traditional energy, such as nature gas, coal, has limited storage and not sustainable, nuclear energy has attracted much attention in the past few decades. Although lots of study has been conducted by thousands of researchers which has attributed to application of nuclear power, there are still some concerns in this field, among which, impurities removal is the most difficult part.

Fluoride salt cooled high temperature reactor (FHR) is one of the most promising Gen IV reactor types. As the name indicates, molten salt is the coolant to serve as the heat exchanger intermedium. In addition, it's inevitable that fission products, i.e. lanthanum, moisture, would leak into the coolant pipe, thus affect the molten salt properties, even degrade reactor performance, therefore, those impurities must be removed without introducing new impurities. In this study, the La_2O_3-LiF-NaF-KF (La_2O_3-FLiNaK) system is used to demonstrate impurity separation into molten fluoride salt. First, solubility of lanthanum oxide in FLiNaK has been measured at different temperatures to understand its dissolution mechanisms. Then, electrochemical experiments with tungsten and graphite as working electrodes were conducted individually to demonstrate the separation of the dissolved oxide from the salt. It has been concluded that tungsten performed well to separate La^{3+}, while failed in the separation of O^{2-}. However, graphite working electrode has succeeded in the removal of La^{3+} and O^{2-}. Finally,

molecular dynamic simulation with first principle was also conducted to further understand the local structure and heat of formation in the molten FLiNaK and La_2O_3-FLiNaK salt.

Acknowledgement

Before joining Dr. Zhang's group, I have worked in a nuclear power plant as an assistant engineer for more than two years, and also as a designer for almost three years. During my five years working in the industry, I never stopped thinking what I really want to do and what kind of person I'd like to be in the future. Thanks to the working experience, it made me realize that my final life goal is to contribute to the scientific research.

Thanks to my parents. They gave me life and brought me up. They have built a model for me with their own well behavior. Even now I often recalled that my father read a book and reviewed his students' homework beside his desk until midnight. Thanks for my parents' encouragement in the past twenty years. I was a very shy and unconfident girl when I was young. I didn't even dare to speak in public until high school. It was my parents who always told me that I was a smart girl and would surely achieve what I pursued in the future as long as I kept working hard and never gave up. Thanks for my parents' support. They always stand behind me no matter what I choose to do. They never force me to make any choices according to their willing. What they often told me was that as long as you like it, it would be the best. They made me think and act independently. When I graduated from Xi'an Jiaotong university with a Bachelor's degree in 2012, I gave up the chance of being admitted as a Master student without examination and chose to work in Hainan nuclear power plant. Although both of them hoped that I could continue to stay at school to obtain a Master's degree first, they never forced me to do that and just told me that as for the choice, there is no good one or a bad one. The only difference is how you would manage your life later. In 2016, I told them I would like to go back to school and study further in the nuclear field. At that time, I have been twenty-six years old, an age that one should think

about getting married and enter the next life stage, but my parents never show any opposition or persuade me to give up the idea of studying abroad. They told me that they just want me to be healthy, happy and could live an easy life, studying abroad alone may be hard, but if it would make me happier and that kind of life was what I wanted, they would always support me. I was so lucky that I could be the daughter of my parents, they love all of me, including virtue and defect. They gave me the best they could afford and allowed me to be a real me. Thanks, father and mother, I love you.

Thanks to Dr. Haghighat. I took his Monto Carlo course and nuclear analysis course in fall of 2017 and spring of 2018. I appreciate his style of giving the lecture which is often full of humor. He encouraged me a lot in his class, and maybe, he even didn't realize or remember the words he said. Whatever, thanks Dr. Haghaighat for the encouragement.

Thanks Dr. Pierson to serve in my Master defense. I took his radiation shielding course in spring of 2018 and learned a lot. I was really impressed by his detailed explanation and well prepared slides in the class. Thanks Dr. Pierson.

Thanks Jianbang Ge for his suggestions on this thesis. Thanks Yafei Wang, Shaoqiang Guo for their suggestions during the experiment operation.

Special thanks to Dr. Zhang. Thanks to give me a chance to join your group and support my research in America. I have made some troubles for you in the past one year, but you never gave up on me. I am full of gratefulness that I could be one of your students. Without your support, I may have dropped out. Thanks so much to believe in me that I could be a good student and give me suggestions on research and life. If I could become a professor in the future as I expected, you are definitely the one that have changed my life at the appropriate time. Thanks so much. You are not only an excellent advisor but also a fabulous writer. I read your poem in Zine.

Actually, I was shocked by your writing ability and creativity on the literature. Not every poet has the magic to use the simple words to arise readers' empathy. Before that I believe there's only one poet named Xiuhua Yu whose works could make tears filled in my eyes. The words in your works are so powerful. It makes me recall the first time that I read the novel "Me and Antiquated Park" written by Tiesheng Shi in high school. Part of that novel was include in my Chinese textbook. I read it again and again with tears flowing out that I cannot control.

Thanks so much, Dr. Zhang.

Table of Contents

List of Figures

List of Tables

List of Abbreviations

FPMD	First Principle Molecular Dynamics
AIMD	Ab Initio Molecular Dynamics
MSR	Molten Salt Reactor
DFT	Density Function Theory
VASP	Vienne Ab-initio Simulation Package
FHR	Fluoride High Temperature Reactor
NVT	Fixed particle Number, Volume and Temperature
PBE	Perdew-Burke-Ernzerhof
GGA	Generalized Gradient Approximation
RDF	Radial Distribution Function
IPMD	Interatomic Potential Molecular Dynamics
PAW	Projector Augmented Wave
NPP	Nuclear Power Plant
ORNL	Oak Ridge National Laboratory
ARE	Aircraft Reactor Experiment
DOE	Department of Energy
MSRE	Molten Salt Reactor Experiment
DMSR	Denatured Molten Salt Reactor
REM	Rare Earth Metal
SINAP	Shanghai Institute of Applied Physics
CAS	Chinese Academy of Sciences

FLiNaK	LiF-NaF-KF
FLiBe	LiF-BeF2
VHTR	Very High Temperature Reactor
ICP-MS	Inductively Coupled Plasma Mass Spectrometry
VHTR	Advanced High Temperature Reactors
CV	Cyclic Voltammetry
CP	Chronopotentiometry
LDA	Local Density Approximation
XRD	X-Ray powder diffraction
CNs	Coordination Numbers
HF	Hartree-Fock approximation

1. Introduction

1.1. Molten Salt Reactor

In order to minimize the impact of nuclear power on the environment and maximize the benefits from the saving of raw materials for nuclear fuel production, the interest in the development of advanced new generation reactor types has engendered a raise. A molten salt reactor (MSR) is a type of nuclear fission reactor in which the primary nuclear coolant and/or the fuel is a molten salt mixture and is designed to operate at high temperature in range of 700 °C – 800 °C. There are roughly two types of molten salt reactor, one is solid fuel molten salt reactors, the other is liquid fuel molten salt reactor. The difference between these two reactors is the reactor fuel. Recently, liquid fuel molten salt reactors have simply been called molten salt reactors. For liquid fuel molten salt reactors, the nuclear fuel can be dissolved in a matrix of molten salt which is heated up in reactor core by fission reaction. This molten salts act as well as primary coolant for the nuclear reactor. Then, heat generated in the core is transferred to a secondary coolant which is also molten salt. The low temperature molten salt will be pumped back to the core, heated up again and begin a new cycle. In case of an accident, the liquid molten salt will be drained into the tank thus the reactor shutdown. This type of reactors represents a very important technology which can achieve the final two goals — significant decrease of radiotoxic waste from the light water reactors for final disposal and effective utilization of raw fuel materials with minimized waste generation.

The development of MSR can be categorized into four eras. The very first MSR research started with the U.S. Aircraft Reactor Experiment (ARE) to support the Aircraft Nuclear Propulsion program, which is a 2.5 MWth nuclear reactor experiment designed to attain a high energy density for use as an engine. In ARE, molten fluoride salt NaF-ZrF_4-UF_4 was used as fuel, while beryllium oxide served as moderation. In the secondary loop, liquid sodium was chosen as the coolant. During this experiment, the reactor kept running for nine days with a peak temperature of 860 °C at Oak Ridge National Laboratory (ORNL) in 1954. An MSR was operated at the Critical Experiments Facility of ORNL in 1957. The experiment lasted for several weeks with the temperature being held constant at 675 °C. Then it comes to the second period during which ORNL lead the study on molten salt reactor experiment (MSRE) through the 1960s. The fuel of the reactor was LiF-BeF_2-ZrF_4-UF_4, moderated by graphite and the secondary coolant is LiF-BeF_2. It went critical in 1965 and ran for four years [1]. The operation temperature reached as high as 650 °C and achieved 1.5 years' full power operation. In the third era, the most important achievement of ORNL was a molten salt breeder reactor (MSBR) design. Fuel was LiF-BeF_2-ThF_4-UF_4 with graphite moderator and NaF-$NaBF_4$. But the MSR program closed down in early 1970s in favor of the liquid metal fast breeder reactor and the program didn't revive until 1976. Finally, in 1980, ORNL proposed the conceptual design of a denatured molten salt reactor (DMSR) with once through fueling which examined the conceptual feasibility of a molten salt power reactor fueled with denatured uranium 235 and operated with a minimum of chemical processing. Theoretically, fueling with low enriched uranium can maximize proliferation resistance. After that, a "30 Year Once Through Design" converted from DMSR was also proposed [2]. It can maintain a very high conversion ratio and excellent uranium utilization without any fuel processing for a full 30 years. However, over the next 30 years, there's no great

advance in the nuclear reactor design. Until in 2002, the molten salt reactor was selected as Generation IV reactor, which contributed to an increase in interest.

1.2. Fluoride Salt Coolant

Based on the concept of MSRs, generally, if the nuclear fuel is dissolved in a matrix of molten salt which is heated up by the fission reaction in the reactor core, the molten salt works as fuel solvent as well as primary coolant. The heat generated in the reactor core will be transferred to a secondary coolant by heat exchanger. Here, the secondary coolant is also molten salt. If the molten salt is used as the fuel solvent, it must meet the following requirements: low neutron capture cross section, low melting temperature, relatively low toxicity, high solubility of fuel materials and corrosion resistance of structural materials. However, if the reactor is loaded with solid fuel and the molten salt just acts as the coolant whose function is to transfer the heat, then the evaluation criteria will focus on the heat performance which indicates that it should have great chemical stability at high temperature, low melting temperature, large specific heat and thermal conductivity.

Fluoride salts are low-volatility fluid with high volumetric heat capacity, melting temperature, and boiling temperature, which is a better choice as coolant of a high-temperature nuclear reactor. In general, the coolants are eutectic binary or ternary mixtures of fluoride salts, such as FLiBe and FLiNaK, among which, FLiBe is a very common primary coolant for FHRs. It was selected for its relatively low neutron absorption cross section and neutronic properties which allowed for negative temperature and void reactivity coefficient of the coolant, which were very important features of critical fission reactors [3]. However, BeF_2 requires special and expensive handling effort due to toxicity, thus making it not a good choice when applied in the

experiments. Therefore, FLiNaK is used as a main alternative for its low toxicity, excellent heat transfer properties and chemical properties similar to those of FLiBe. The only disadvantage of this molten slat is that KF has large parasitic capture cross section which is not good to act as fuel solvent.

In addition, one main characteristic of fluoride molten salt is high melting point which means the reactor have to be equipped with external heating source. However, the high melting point can be also an important advantage of the molten salt coolant. If an accident happens, e.g., LOCA, the coolant leak out can be solidified in a short time thus minimizing the radiation proliferation. Both FLiNaK and FLiBe have melting point lower than the operation temperature, higher heat capacity and density which are required for excellent heat transfer. The only difference is that the FLiBe is chosen as fuel solvent due to its desirable nuclear cross section, while FLiNaK serves as coolant of the second loop for its high heat capacity.

1.3. Molten Salt Reactor Challenges

Molten salt reactors can load either solid fuel or liquid fuel. Both high temperature, fluoride salt coolant reactors (FHR) and Advanced High Temperature Reactors (AHTRs) use solid fuel [4]. The advantage of the solid fuel with molten salt coolant reactors over liquid fuel reactors is that the cladding of the solid fuel adds an extra barrier to fission product release and the component of salt as a coolant is much simpler, while molten salts serve as the second level protection shielding. Finally, the reactor vessel and rector building serve as the third level protection. But there is one drawback of solid fuel which is that the fuel burn up will remain at the modest levels and the structure of the solid fuel will degrade upon irradiation.

For the MSRs with liquid fluoride fuel, the fuel is dissolved in fluoride molten salts. They circulate rather quickly through the active zone of the reactor. With the reactor operation and burn up, the amount of fission products in the fluoride salt will increase which makes the feeding with the fresh fuel necessary. In addition, the main fuel stream should also be reprocessed to remove fission products to maintain the suitable ratio between fission material and fission products in the reactor core. One of the most important species to be cleaned is fission products which may influence the salt properties and can also be radioactive source terms. The goal of salt processing is to satisfy the constraints for smooth reactor operation while minimizing the waste streams. The implementation of clean up system is needed especially for the actinide-lanthanide separation [5], due to their lower neutronic captures which could decrease the reactivity balance [6].

In this study, the research focus on the FHRs. If fuel failure happens, e. g., a rupture in the fuel cladding that allows the fission products, either in the form of dissolved radioisotopes or hot particles to enter the primary coolant, fission products will contaminate the primary fluoride salt coolant. Also, it's possible that the moisture can leak into the coolant, thus resulting in oxygen impurity which is the main corrosion source to coolant pipes. Therefore, FHRs will have primary coolant cleanup system installed to mitigate the contamination from leaking fuels and ingress of moisture. Moreover, high temperature fluoride salts could dissolve oxide protective layer on structural alloys which would also introducing oxygen impurities into molten salts. It is better that the structural alloys for FHRs are thermodynamically stable to protect against corrosion from the primary coolant rather than relying on a protective oxide coating. To handle these challenges and explore techniques to solve the corresponding issues, the present study is done to

focus on the behaviors of lanthanum oxide in the fluoride molten salt, including its solubility and electrochemical separation.

1.4. Solubility of Lanthanide Oxide

Solubility of rare earth oxide in fluorides and in-depth understanding of the dissolution behavior are both of fundamental and engineering importance for the design of the fuel clean up system. In this study, lanthanide and oxygen elements are regarded as the impurities which should be removed from the molten salt. Hence, the lanthanum oxide will be dissolved into the fluoride molten salt serving as impurity. As for the solubility of lanthanum oxide, there are only few research on this topic. Even worse, there is inconsistency between results from different studies which makes the access to reliable data more difficult.

Solubility of rare earth oxide is mainly affected by four different factors which are temperature, rare earth fluoride content, alkali metal fluoride content and alkali earth metal fluoride content. First, temperature is an important factor in studying a thermodynamic property. It has been clear that the solubility of rare earth oxides increases with temperature. The dissolution of rare earth oxide into the fluoride can be simplified as an endothermal reaction. The equilibrium would move to the direction that favors the dissolution of rare earth oxide at higher temperature thus obtain higher solubility of rare earth oxides in molten salt. Secondly, a corresponding rare earth metal fluoride is usually added into the fluoride melt used to dissolve the rare earth oxide [7]. Most of the published data conclude that the rare earth solubility increases with the adding of rare earth fluoride in the molten salt [7]. In this dissolution process, the long range order in the rare earth oxide is destroyed by the oxygen ions and the ion complex of rare earth metal fluoride form oxyfluoride function group which is beneficial to rare earth oxide dissolution. Third, the

alkali fluoride material will contribute to lowing the melting point of the electrolyte and improving electrical conductivity. The radius of alkali metal ions is always much smaller than the rare earth metal ions thus resulting in lower resistance of its movement and higher mobility in the melt. The conductivity is closely related to the moving speed of the alkali metal ions in the melt. Therefore, the melts with higher concentration of alkali metal ions would have relatively higher conductivity. Finally, the alkali earth metal fluoride can further lower the melting point of the molten salt mixture as well as limiting the evaporation of alkali metal fluoride and lowering the melt viscosity. It has been confirmed that the addition of alkali earth metal fluoride can prevent the evaporation of alkali metal fluoride [8]. However, as for its influence on the solubility of rare earth oxide, in some cases, the effect is positive, while sometimes negative, there is still no accurate conclusion.

Generally, two methods are mainly applied to study the solubility. One is thermal analysis in which the temperature of phase transitions is determined based on the cooling and heating curves of the heating molten salt mixture [9]. That is, primary crystallization temperature and eutectic temperature of different lanthanide oxide fraction were obtained first. Then, the phase diagram can be built based on these two kinds of phase transition temperatures. This method is relatively easy to implement, however, as the phase diagram has a strong relation with the phase transition temperature, if the temperature obtained from the experiment has large deviation, it would result in larger error on the solubility. Therefore, another method called isothermal saturation is applied [10]. An amount of lanthanum oxide exceeding the expected solubility was added in the fluoride salt. The salt mixture would be heated for enough long time to make the whole system be equilibrium. Finally, lanthanum concentration in the fluoride molten salt was determined by the Inductively Coupled Plasma Mass Spectrometry (ICP-MS). Theoretically, as long as the system

reach stable after heating with long time, the final lanthanum concentration can be used to calculate the corresponding solubility. Compared with the thermal analysis, this method is much more reliable which only rely on the ICP-MS. The only concern is that when the system will reach equilibrium. Therefore, the second method is applied to explore the solubility of La_2O_3 in molten FLiNaK in this study.

1.5. Electrochemical Measurement Methods

Electrochemistry is the branch chemistry concerned with interrelation of electrical and chemical effects. It can deal with the study of chemical changes caused by the passage of an electric current and the production of electrical energy by chemical reactions. Electrochemical measurement on chemical system can be applied in a variety of fields, such as obtaining thermodynamic data about a reaction, analyzing a solution for trace amounts of metal ions or organic species [11].

In the field of molten salt reactor nuclear fuel cycle, it requires an online clean up processing of fuel to remove fission products, especially lanthanide which have poisonous effect on the nuclear reactions in the core of reactor. Therefore, lots of studies have been done to develop on-line pyrochemical reprocessing technology, among which, the electrochemical separation method is highlighted. It represents one of the most promising methods for the separation process, together with molten salt extraction techniques, which can be applied to separate the fission products from fission material in molten fluoride salt [12]. In fluoride molten salt system, separation of fission products, e.g. uranium and lanthanum, can be categorized into two types. First, if the fluoride carrier melt is electrochemically stable enough, it is possible to deposit the element in metallic state. Otherwise, the fluoride melt is insufficiently electrochemical stable, a reactive

cathode electrode made of materials which can form alloy with the metal supposed to be deposited can be used. The alloy reaction can shift the deposition potential in a favorable direction thus realizing the separation of interested element from the system. On the other hand, the formation of alloy improves the adhesion of the deposit [13].Since the reaction process on the surface of electrode can be characterized by electrochemical analysis, the cyclic voltammetry and chronopotentiometry are applied in the present study to identify if the interested elements could be separated from the molten salt.

1.5.1. **Cyclic Voltammetry**

Cyclic voltammetry is an electrochemical technique which can measure the current in an electrochemical cell with the applied potential. It is performed by cycling the potential of a working electrode while the resulting current is measured in the forward and reverse directions once or several times. In the cyclic voltammetry experiments, the working electrode potential is ramped linearly vs. time. After the set potential is reached, the potential on the working electrode will be ramped in the opposite direction to return to the initial potential. The obtained plot shows the relationship between the current and the applied voltage.

A standard cyclic voltammetry experiment employs a cell fitted with three electrodes: working electrode, counter electrode and reference electrode which is usually called three-electrode setup. The potential range that can be applied during the experiment is determined by the solvent, electrolyte and material composition of the working electrode. During a cyclic voltammetry experiment, the electrodes are immobile and sit in unstirred solutions, which makes the diffusion controlled peak possible. Moreover, the still unstirring solution also allows some amount of analyte to remain and display further redox activity after reduction and oxidation. It is common

that the reduced or oxidized analyte species would precipitate out onto the electrode. This deposition layer can insulate the electrode surface, display its own redox activity in the subsequence scans. Therefore, it is often necessary to clean the electrode between scans.

In electrochemistry, Nernst equation is the most important equation. The fundamental expression simply specifies the relationship between the potential on the working electrode vs. reference electrode and the concentration of the two species involved in the redox reaction at the electrode. Assuming that the following reaction *(1)* follows the Nernst equation:

$$O + ne^- \leftrightarrow R \tag{1}$$

$$E = E^{0'} + \frac{RT}{nF}\ln(\frac{C_O}{C_R}) \tag{2}$$

Where $E^{0'}$ is the apparent potential for the couple involving O and R, C_O is the concentration of the reactant O, while C_R is the concentration of the production R.

In cyclic voltammetry, for a typical reversible system, the peak current is given by [11],

$$i_p = 2.69 \times 10^5 \times n^{3/2} A D^{1/2} v^{1/2} C \tag{3}$$

The cathode peak potential E_p is given by,

$$E_p = E_{1/2} - 1.109\frac{RT}{nF} \tag{4}$$

Because the peak is somewhat broad, the peak potential may be difficult to determine. Sometimes it is more convenient to report the potential at $\frac{i_p}{2}$, which is called the half-peak cathode potential $E_{p/2}$ given by,

$$E_{p/2} = E_{1/2} + 1.09\frac{RT}{nF} \quad (5)$$

Combine *(4)* and *(5)*, then,

$$|E_p - E_{\frac{p}{2}}| = 2.2\frac{RT}{nF} \quad (6)$$

Thus, for a reversible wave, E_p is independent of scan rate and i_p is proportional to $v^{1/2}$. Hence, depending on what is already known about a given system, one could determine the concentration, the diffusion coefficient, the number of the transferred electrons per molecule of analyte oxidized or reduced, the redox potential for the analyte from a single experiment.

1.5.2. **Chronopotentiometry**

In chronopotentiometry, a current pulse is applied to the working electrode and the resulting potential is measured against the reference electrode as a function of time. If a constant current is applied to the electrode resulting in the eletroactive species to be reduced or oxidized at a constant rate. The electrode potential accordingly varies with time as the concentration ration of reactant to product changes at the electrode surface [14]. After the reactant concentration drops to zero at the electrode surface, there will be no sufficient reactant to accept the electrons forced by the current. The potential will then be sharply changed to more cathodic or anodic values. Chronopotentiometry is principally concerned with the measurement of the transition time τ, which can be related to the kinetic parameters of the process involved. In an irreversible anodic wave, the relation between potential, transition time is given by [25],

$$E = E^{0'} + \left(\frac{RT}{\alpha n_\alpha F}\right) \ln\left[\frac{2k^0}{\pi D}\right] + \left(\frac{RT}{\alpha n_\alpha F}\right) \ln(\tau^{\frac{1}{2}} - t^{\frac{1}{2}}) \quad (7)$$

Where $E^{0'}$ is formal potential of the reaction, k^0 is standard heterogeneous rate constant. Meanwhile, the applied current density is given by Sand's equation [15],

$$\frac{i\tau^{\frac{1}{2}}}{C} = \frac{nAFD^{1/2}\pi^{\frac{1}{2}}}{2} \quad (8)$$

Where A is the electrode surface area, C is the bulk concentration of the analyte, and D is the diffusion coefficient. If the reactions involve the material adsorption on the electrode surface. The electroactivity of the materials will have effects on the potential response. If it is not electroactive, $i\tau^{\frac{1}{2}}$ will decrease due to the fact that less time is needed at higher current for the electroactive materials to penetrate the layer.

Cottrell equation is another equation that can also be used in electrochemical analysis, especially in chronoamperometry which is given by,

$$i = \frac{nFACD^{1/2}}{\pi^{\frac{1}{2}} t^{\frac{1}{2}}} \quad (9)$$

Comparing these two equations, the advantage of Sand's equation is that it is appropriate for both planar and spherical electrodes, in other words, τ is independent of diffusion form and electrode surface. While for Cottrell equation, it can only be applied with diffusion controlled current for a planar electrode at a constant potential. The Sand's equation and Cottrell equation

are also related in that both of them can be used to calculate the diffusion coefficient. But in Sand's equation, the transition time τ shows linear relation with D, while the peak current i is related with $D^{1/2}$.therefore, better precision can be obtained with Sand's equation [16].

1.6. First Principle Molecular Dynamics Simulation

First principle molecular dynamics simulation is also called ab initio simulation. It's applied on the atomic modelling such as local ionic structure calculations and quantum molecular dynamics. In this study, the model would be built with Vienna Ab initio Simulation Package (VASP). In the molecular dynamics simulation with VASP, the solution to the Schrodinger equation is either estimated by the density functional theory (DFT) or the Hartree-Fock (HF) approximation.
In VASP, there are four main input files which are INCAR, KPOINTS, POSCAR and POTCAR shown in Figure 1-1.

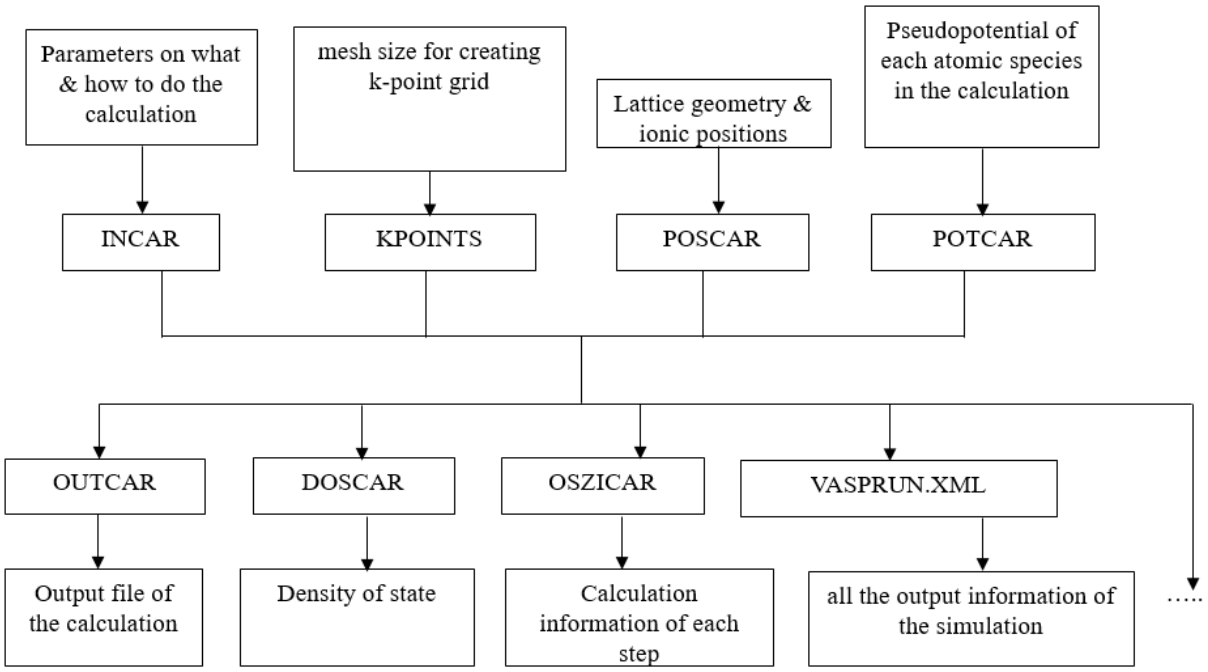

Figure 1-1 Flow chart in VASP simulation calculation

After the running, four main different output files could be obtained which are OUTCAR, DOSCAR, OSZICAR and VASPRUN.XML. Based on these simulation results, the structure information, e.g. first peak radius and first shell coordination number, density of state and transport properties, e.g. self-diffusion coefficient could be obtained after corresponding analysis.

In this study, local ionic structure of molten salt and effect of oxygen ions on the properties of molten salt are interested. The simulation box of FLiNaK and FLiNaK-La_2O_3 were built with VASP. In addition, enthalpy of formation in the molten salt mixture were calculated as well as Gibbs free energy of some solid state salt, e.g. LaF_3 and LaOF.

2. Solubility Study of La_2O_3 in Molten FLiNaK Salt

2.1. Introduction

In high temperature fluoride molten salt reactors equipped with solid fuel, it is possible that the fission product, such as lanthanum, will enter the molten malt thus forming a potential threaten to the nuclear reactor operation, e.g. it may affect the thermal and/or transport properties of the molten fluoride salt. Meanwhile, moisture coming from the coolant also has a chance to leak into the molten salt which will result in the introduction of oxygen ions into the reactor. In addition, high temperature could dissolve oxygen ions of the structure materials to the coolant.

As it is well known, the strong oxidation properties of oxygen make it one of the most important sources attributing to the nuclear structure corrosion. Therefore, fission products and those oxygen ions must be removed from the molten salt to make sure safe reactor operation and extent the lifetime of the reactor structures. Among all kinds of separation methods that proposed in recent years, one promising way to separate the fission products and oxidation impurities is highlighted, which is electrochemical method with sacrificial working electrode. The impurities formed in the fluoride molten salt can be separated on the basis of their individual different electrochemical properties, e.g., formation of alloys, electrochemical deposition potential.

This study is part of a project dealing with the electrochemical separation of impurities leaking into the primary molten salt coolant in the high temperature molten salt reactors with solid reactor fuel pellets. Here, lanthanum oxide dissolved in the molten fluoride salt was chosen as an example. It will demonstrate the solubility and phase patterns at different temperatures to mimic the actual operation condition in real reactor operation. As for the solubility of lanthanum oxide

in the molten fluoride salt, studies in this field is still limited. Until now only a few studies have been done. In 2008, Ambrová., et al [9] studied the solubility of lanthanum oxide in molten alkali fluorides with thermal analysis and concluded that the solubility of La_2O_3 in molten FLiNaK is 1.5 mol% which was lower than in pure LiF and NaF but higher than in KF. In R. M. Wheat's study [10], the isothermal saturated method was applied. It was demonstrated that the solubility of lanthanum oxide, samarium oxide and holmium oxide increased with the temperature and showed linear relationship between the nature logarithm of the solubility and the reciprocal temperature. In 2014, another study was conducted by X. L. Guo [7]. In his work, the available data on the rare earth oxide solubility in molten fluoride salt was summarized and analyzed which proposed that the rare earth oxide solubility increases with rare earth metal fluoride salt. However, the solubility of lanthanum oxide in these studies didn't accord with each other which indicated that more research is still needed to further understand the solubility mechanism of lanthanum oxide in molten fluoride salt. Besides the lanthanum oxide, there have been several studies on other lanthanide oxides which could give us a glance in this field and provide some references on the study of the lanthanum oxide. In E. Stefanidaki's research on the electrodeposition of neodymium from LiF-NdF_3-Nd_2O_3 melts, it was proposed that the neodymium oxyfluorides would be formed if neodymium oxide was added to the molten LiF [17]. S. I. Berul and N. K. Voskresenskaya studied the solubility of CeO_2 and Sm_2O_3 in molten NaF-KF. They found that samarium oxide could form SmF_3 and SmOF during dissolution and there was also Na_3SmF_6 existed in NaF-KF melt [18].

2.2. Experimental Setup

In this study, 4 experiments at 4 different temperatures are. As is well known, the operation temperature of fluoride high temperature reactors is between 600°C and 800°C. Therefore, the experiment temperature in this study was set at 600°C, 650°C, 700°C and 750°C respectively to mimic the real operation condition in the reactors. LiF (BioUltra, ≥99.0%, Sigma), NaF (ACS regent, ≥99.0%, Sigma-Aldrich), KF (ACS regent, ≥99.0%, Sigma-Aldrich) and La_2O_3 (≥99.9%, Aldrich) were used in this experiment. Without special noting, all the operations were done in the glove box with <2.5ppm O_2 level and <1.0ppm H_2O level. 1.5000g La_2O_3 was placed on the bottom of the Nickle crucible which served as salt container first. After that, 14.6054g LiF, 5.8472g NaF, 29.5474g KF were mixed well before adding into the Nickle crucible which would lay on the top of La_2O_3 to ensure the result accuracy in the experiment. In addition, the furnace was preheated at 200°C for 1 hour to remove possible moisture and other impurities probably hidden in the furnace parts. Then, alumina safety crucible and Nickle crucible with salt inside were placed into the furnace. The temperature was kept at 200°C for another 2 hours to ensure that the moisture in the salt and other low boiling points impurities could be evaporated in this process. The heating temperature was increased to 400°C 2 hours later to remove those impurities with higher boiling points. Finally, after totally 5 hours' impurities removal process, the heating temperature would be set at the goal temperature, e. g., 600°C, 650°C, 700°C and 750°C, and kept for different days as shown in Table 2-1 . During the heating process, samples were taken at different time for Inductively Coupled Plasma Mass Spectrometry (ICP-MS) to analyze the on-site La concentration in the molten salt. Moreover, the ICP-MS samples taken each time were controlled at about 0.01g±0.005g to minimize the effect of sample mass

measurement variance on the La concentration. The ICP-MS samples were taken at the specific intervals as shown in Table 2-1.

The samples of the molten salt were also analyzed by the X-Ray powder diffraction (XRD) (PANalytical X'Pert PRO, Cu-Kβ, $\lambda = 1.387$Å) from 20-95° 2θ to determine the phase patterns.

Table 2-1 Solubility Experiment information

Heating temperature	Heating time	Interval of samples taken
°C	Hours	Hours
600°C	384	6
650°C	336	6
700°C	73/282	6
750°C	336(167+169)*	6

*Note: In the experiment at 750°C, the salt mixture was heated for 167 hours first to obtain the ICP results, then continued to be heated for another169 hours to obtain ICP results.

2.3. Results and Analysis

In the experiments, it was found that there was still a large amount of insoluble material on the bottom of the crucible as shown in Figure 2-1, even after being heated for 384 hours. Therefore, XRD analysis was done to identify the phase patterns of the insoluble material and the melt mixture. As shown in Figure 2-2 which represents the phase patterns of the insoluble materials on the bottom, the sample consists LaOF and undissolved La_2O_3 besides FLiNaK. The formation of LaOF can be described by the reactions *(10), (11), (12)* and the corresponding Gibbs free

energy of the reaction is also calculated which demonstrate that the reaction between La_2O_3 and alkali eutectic happens in the order of LiF, NaF and KF.

$$La_2O_3 + 2LiF = 2LaOF + Li_2O \quad (10)$$

$$\Delta G_1 = -1141.05kJ$$

$$La_2O_3 + 2NaF = 2LaOF + Na_2O \quad (11)$$

$$\Delta G_2 = -1048.99kJ$$

$$La_2O_3 + 2KF = 2LaOF + K_2O \quad (12)$$

$$\Delta G_3 = -1005.11kJ$$

In addition, XRD phase patterns shown in Figure 2-3 contains the same components as those in the insoluble materials which are a small amount of LaOF, La_2O_3 and large amount of FLiNaK. Known that the sample mass of the insoluble materials and the melt salt taken for the XRD analysis are almost the same (0.02706g and 0.02699g), comparing the peaks of LaOF and La_2O_3 in Figure 2-2 and Figure 2-3, it was found that the peak intensity of those two components in the insoluble materials are much stronger than that in the salt melt. As for the stronger peak intensity of the La_2O_3, it is not difficult to understand that it results from the large quantity of undissolved La_2O_3 accumulated on the bottom due to its higher density than FLiNaK. While for the stronger peak of LaOF, since the sample was taken during the heating process before the experiment completed and then quenched to keep the initial crystal structures, if LaOF is easy to dissolve in the molten fluoride salt, most of it should exist in the melt, not on the bottom. Therefore, it's possible that most of LaOF formed in the reactions of *(10)*, *(11)* and *(12)* would deposit on the

bottom and only a small amount of LaOF dissolved into the melt which would contribute to the La concentration increasing in the system.

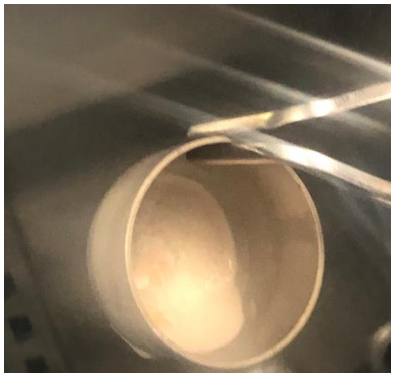

Figure 2-1 Insoluble material on the bottom

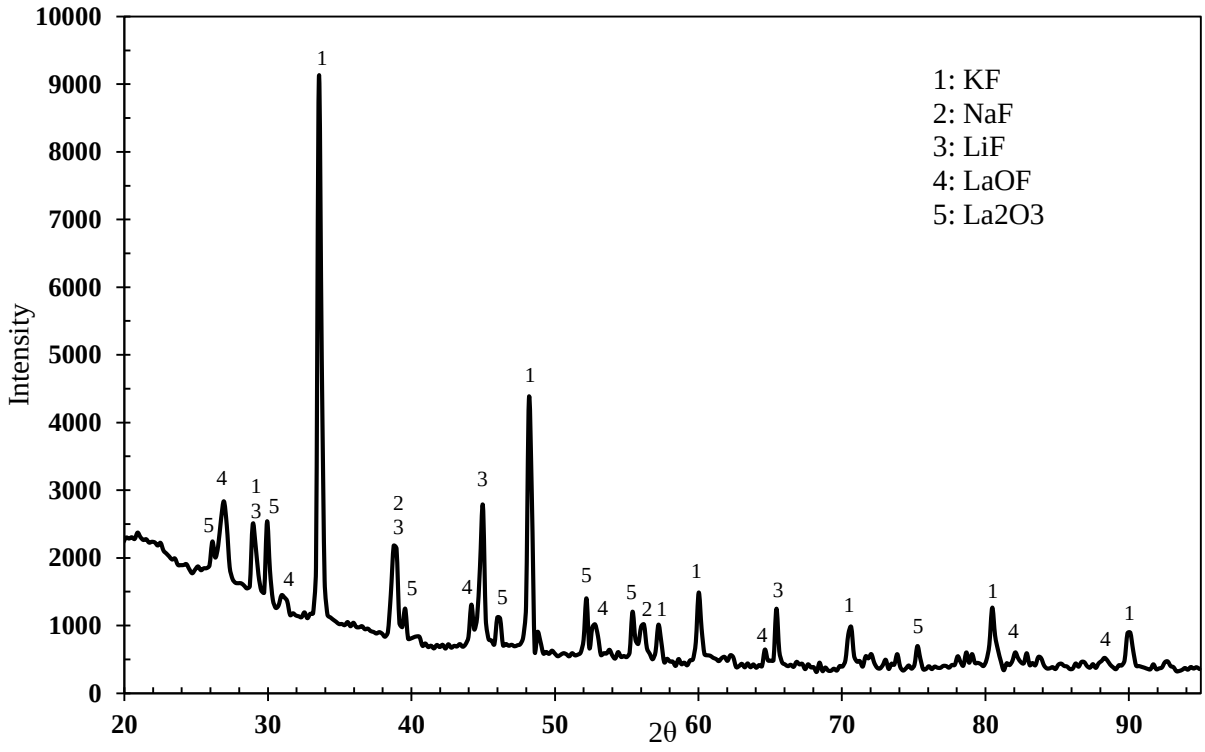

Figure 2-2 XRD of the insoluble materials on the bottom

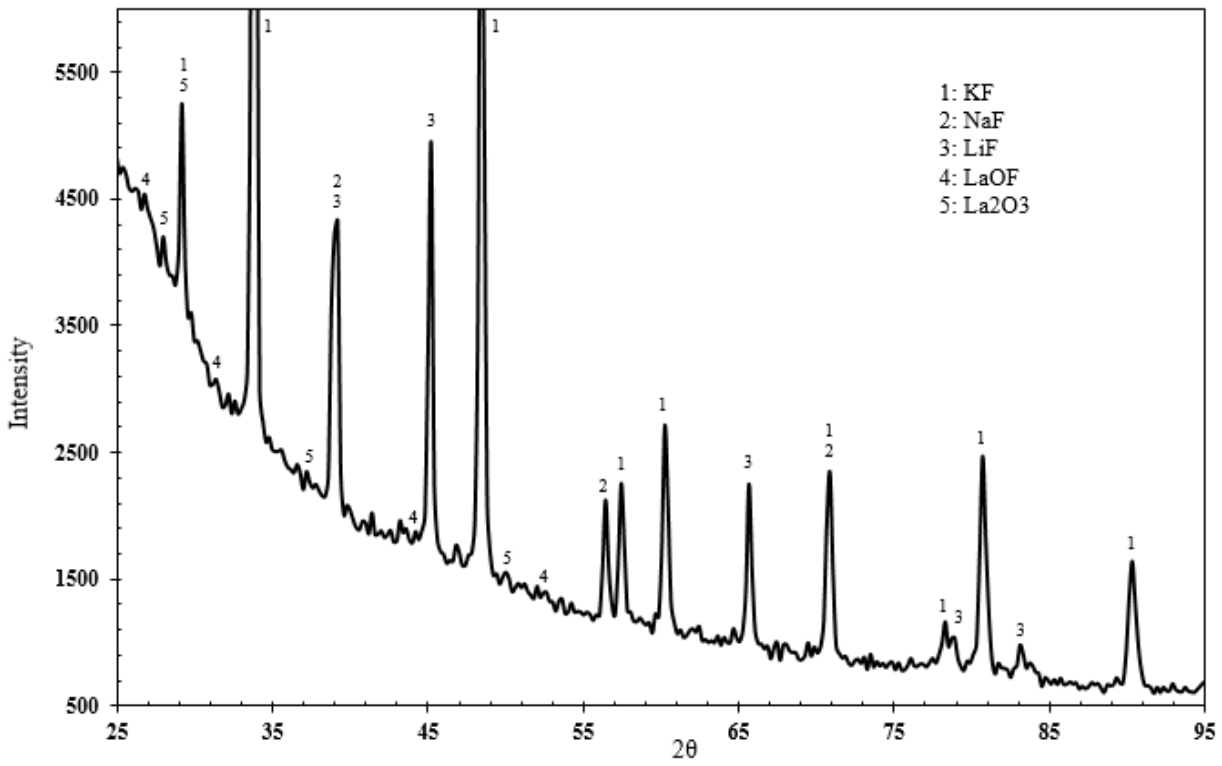

Figure 2-3 XRD of melting salt during heating process

The ICP-MS analysis results at different temperatures are shown in Figure 2-4 and Figure 2-8. La concentration is less than 0.04% both at 650°C and 600°C, while the concentration is between 0.04% and 0.1% both at 750°C and 700°C, which demonstrate that the solubility of lanthanum oxide is actually much smaller than those reported by M. Ambrová [1] and R. M. Wheat [2]. As for the La concentration at 650°C and 600°C shown in Figure 2-4, both of the La concentration at these two different temperatures are stable in terms of heating time, while for the La concentration at 750°C, there are severe fluctuation comparing with the results at 650°C and 600°C. Since the molten salt mixture have been kept at the corresponding constant temperature, it's assumed that the whole system could be regarded as equilibrium. Therefore, the final La concentration could represent the corresponding solubility at each temperature as shown in Table 2-2. The dependence of reciprocal of temperature in K and the natural logarithm of solubility in

mole fraction is shown in Figure 2-7. Without considering the data at 750°C, it shows linear relationship in *(13)*, while for the data at 750°C, it may result from the phase change in the solution during heating process.

$$lnS = -\frac{8208.8}{T} - 1.0614 \qquad (13)$$

Where S: solubility in mole fraction, T: temperature in K.

It is known that the melting point of FLiNaK is 454°C and will increase due to the addition of Lanthanum oxide. But considering that the amount of the La dissolved in the melt is very small according to the results in Table 2-2, the magnitude of the increasing may be neglected which means that the 4 experiment temperatures in this study will be greatly larger than the melting point of the mixture FLiNaK- La_2O_3. Therefore, it is unavoidable that there will be evaporation phenomenon occurred during the heating process. As showed in Figure 2-5, there is no visible trace of evaporated salt on the crucible surface at 600°C, then a small amount of salt can be observed on the surface when the temperature goes up to 650°C. Finally, if the heating temperature is set at 700°C and 750°C, the evaporated salt can even form large salt spots which demonstrate the sever evaporation during the heating process. Since the evaporation only occurs at higher temperature, it's possible that the fluctuation shown in Figure 2-4 could result from that.

Since the data at 750°C in Figure 2-4 only covers the first 167 heating hours, another Figure 2-8 with longer heating time is also shown. A turning point A located between 150hrs and 170hrs is observed after which the curve goes up. Here, if combining this fact with the evaporation phenomenon, an assumption of supersaturated solution is proposed. As is known, the dissolution

of La_2O_3 in molten FLiNaK is a physical-chemical interaction, among which, one of the mechanism is built on the equilibrium process between solid La_2O_3 and La^{3+}, O^{2-} ions given by,

$$La_2O_{3(solid)} \overset{K}{\leftrightarrow} 2La^{3+} + 3O^{2-} \quad (14)$$

Another one is the chemical reaction between the fluoride salt and lanthanum oxide which is given by,

$$La_2O_3 + 2MF = 2LaOF + M_2O \quad (15)$$

$$LaOF \leftrightarrows LaO^{+} + F^{-} \quad (16)$$

$$LaO^{+} \leftrightarrows La^{3+} + O^{2-} \quad (17)$$

Where M is Li, Na, K.

And the equation *(16)* and *(17)* can be combined and given by,

$$LaOF \leftrightarrows La^{3+} + O^{2-} + F^{-} \quad (18)$$

Since the temperature was stable during the heating process, the equilibrium of La dissolution in the molten salt could not be undermined. Therefore, it was assumed that only materials related to alkali elements were evaporated to steam, then cooled on the outside surface of the nickel crucible to form the salt spots after the furnace was turned off and the temperature decreased, while the La element that has already been dissolved in the evaporated molten salt was still remained in the solution thus the super-saturated solution of La was formed. As more sever evaporation occurred, more La would be left over in the solution which shown in Figure 2-8 was

that the La concentration increased after the turning point A and then kept stable when more La can no longer be dissolved in the molten salt.

The XRD analysis of the evaporated salt was done to identify the components in the salt. As shown in Figure 2-6, there is no LaOF or La_2O_3 present in this sample and only FLiNaK and the corresponding alkali oxide produced in *(10)*, *(11)*, *(12)* were identified as expected thus further confirm the assumption on the super-saturated solution.

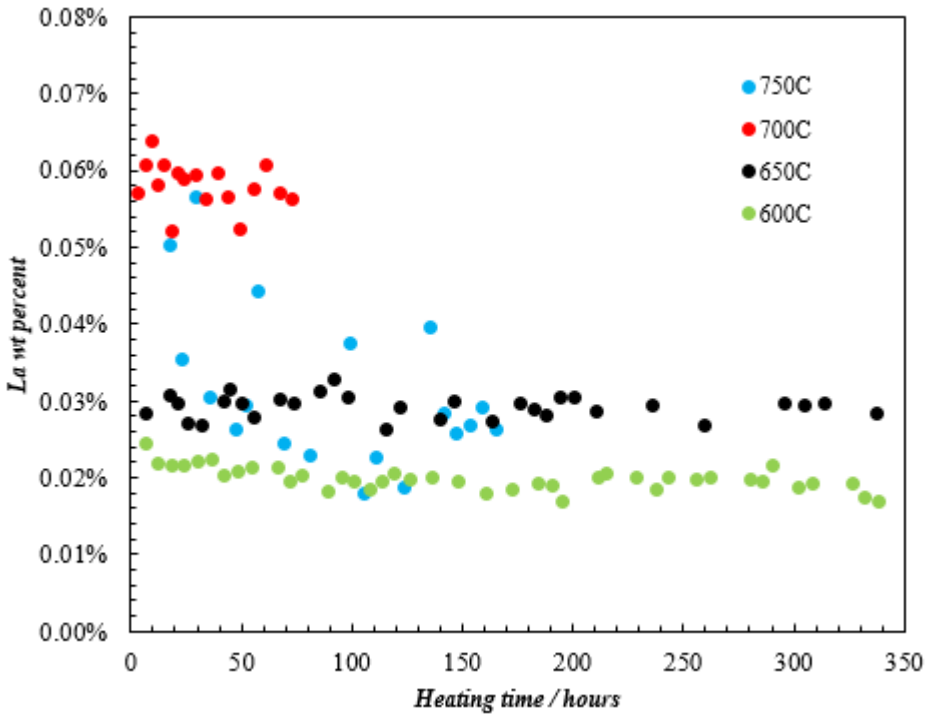

Figure 2-4 La concentration distribution at 600°C, 650°C , 700°C and 750°C

Figure 2-5 Evaporation Phenomenon at different temperatures, from left to right, 600°C, 650°C, 700°C, 750°C

Table 2-2 La concentration and La_2O_3 solubility at 600°C, 650°C, 700°C, 750°C

	Heating Temperature			
	600°C	650°C	700°C	750°C
La Concentration (Weight percent)	0.02% $\pm$ 0.000231%	0.0293% $\pm$ 0.000273%	0.0528% $\pm$ 0.00359%	0.0422% $\pm$ 0.00288%
La_2O_3 Solubility (Mole Fraction)	2.9729 $\times 10^{-5}$% $\pm$ 0.0000343%	4.3557 $\times 10^{-5}$% $\pm$ 0.0000405%	7.8508 $\times 10^{-5}$% $\pm$ 0.000534%	4.6962 $\times 10^{-5}$% $\pm$ 0.000571%

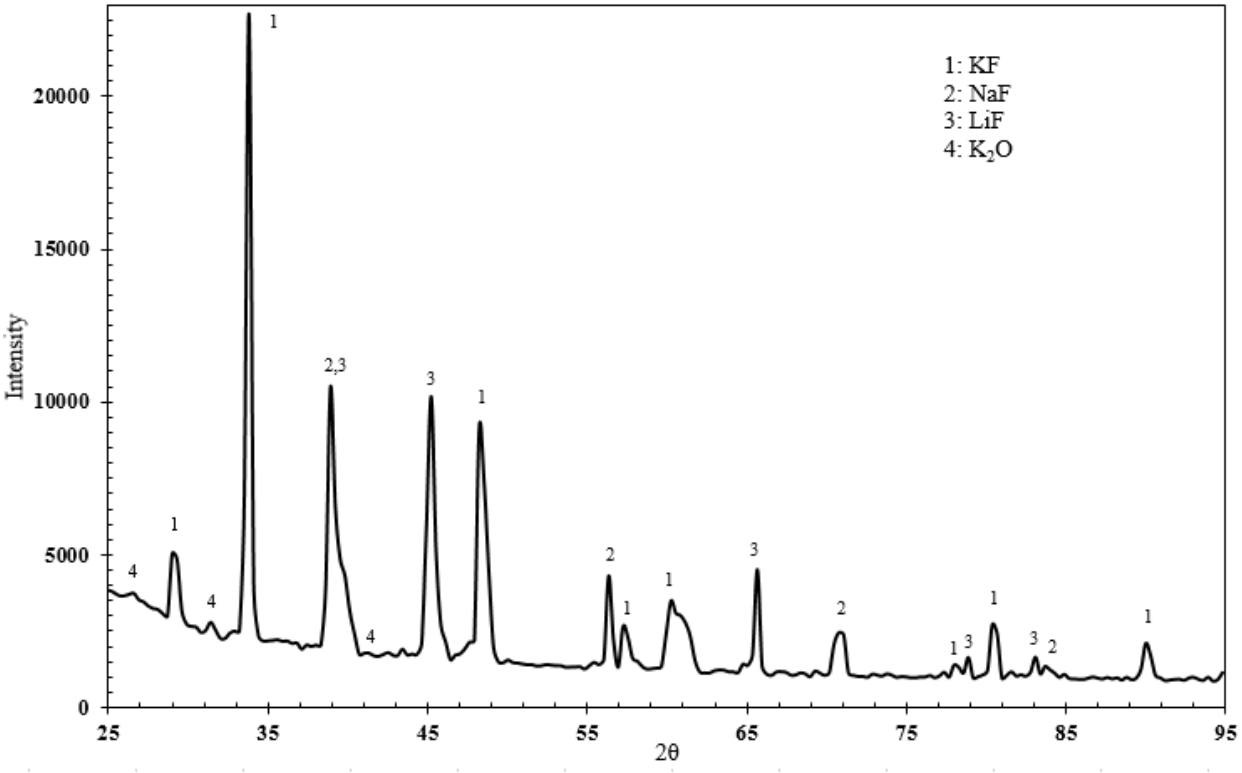

Figure 2-6 XRD of evaporated salt on the surface of the crucible

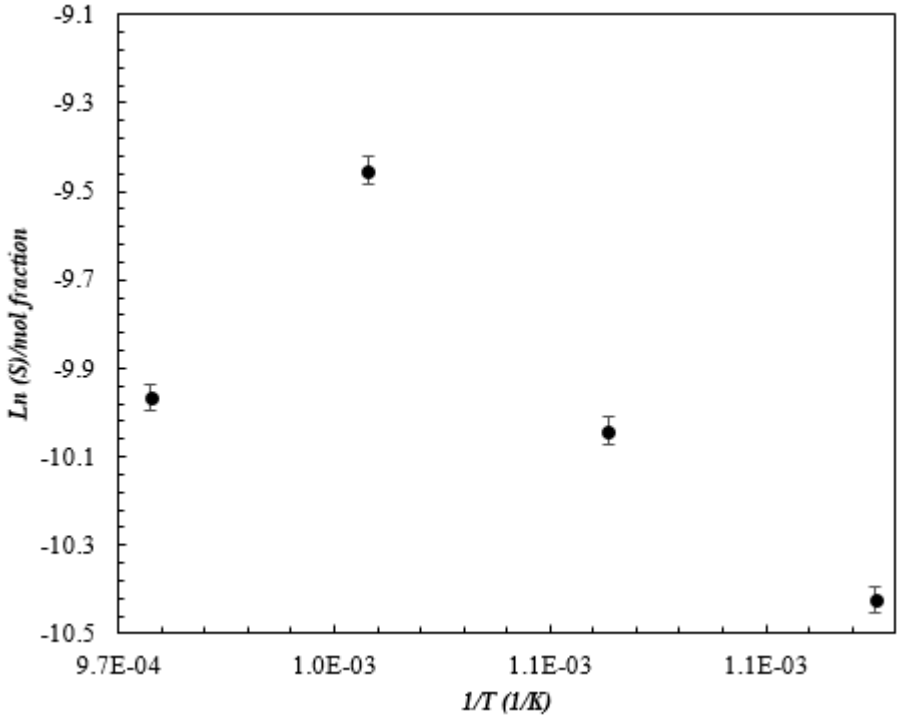

Figure 2-7 relationship between natural logarithm of solubility and reciprocal of temperature in Kelvin

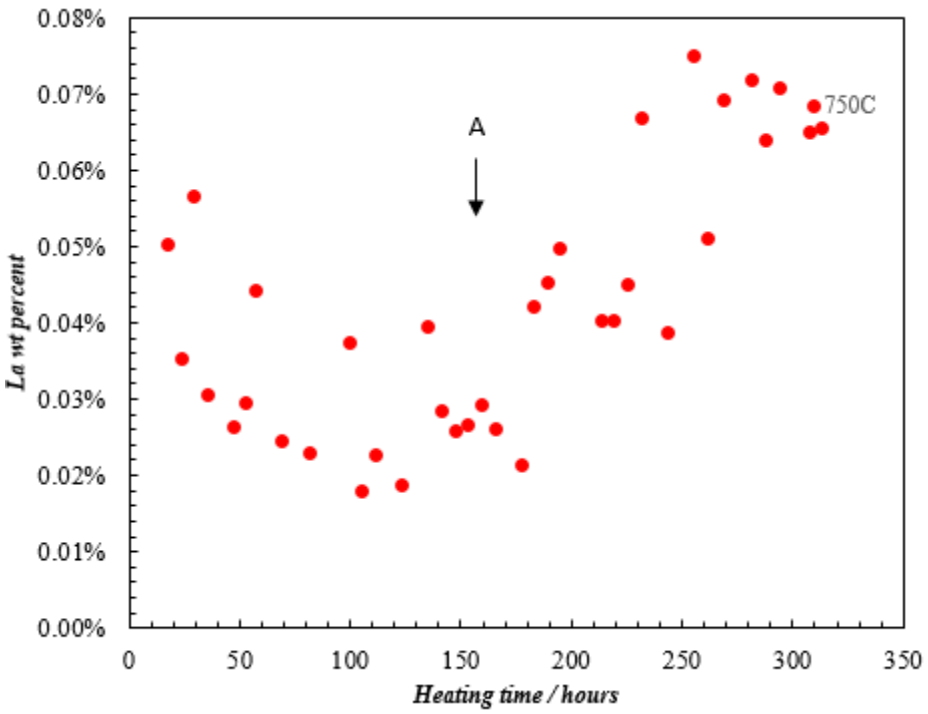

Figure 2-8 La concentration distribution at 750°C

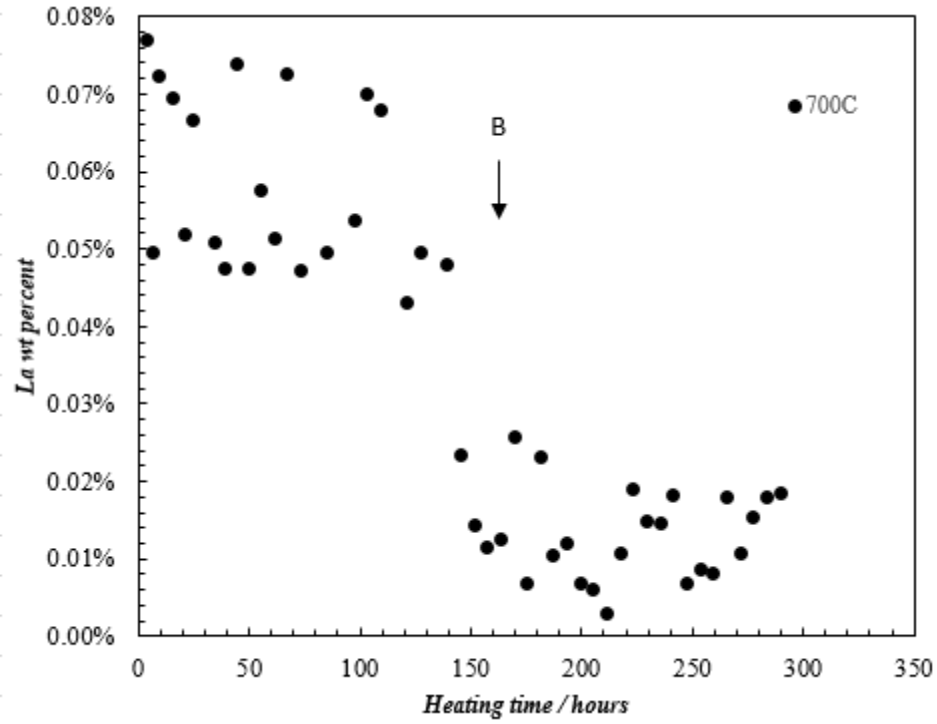

Figure 2-9 La concentration distribution at 700°C

As for the experiment at 700°C, since it only lasted for 72 hours in Figure 2-4, another experiment operated for 282 hours was conducted. The corresponding La concentration curve is shown in Figure 2-9. Comparing with Figure 2-8, there is still fluctuation which may result from the evaporation as discussed before.

In addition, the La concentration decreases sharply after turning point B and keeps at as low as $0.0132\% \pm 0.00127\%$ after being heated for 220 hours which is beyond expectation. The super-saturated solution of La could not be applied to explain the La concentration curve trend shown in Figure 2-9, which, in the other hand, indicates that the complicated dissolution mechanism of La_2O_3 in molten fluoride salt deserves more studies.

2.4. Conclusions and Future work

The solubility of lanthanum oxide in molten fluoride salt has been studied in this work. Without considering the second experiment at 700°C and 750°C, the La_2O_3 solubility increases with temperature and there is a simple linear relationship between the nature logarithm of the solubility in mole fraction and the reciprocal of the temperature in Kelvin. It was also found that most of LaOF formed in reaction *(15)* could deposit on the bottom due to its higher density. Moreover, the evaporation does exist during the heating process and it becomes more sever with heating temperature increasing, thus leading to the formation of La super-saturated solution which makes the La concentration increase after turning point A shown in Figure 2-8. However, although the super-saturated solution theory performs well on the solubility study at 750°C, there is still one issue existed that it cannot be applied to explain the La concentration curve trend with longer heating time at 700°C. Therefore, more studies are urgent to be conducted in the future to further explore the dissolution mechanism of La_2O_3 in molten FLiNaK salt.

3. Electrochemcial Separation Study of La_2O_3 in Molten FLiNaK Salt

3.1. Introduction

As one of the promising type reactor among all kinds of molten salt reactor, fluoride salt cooled high temperature reactor has attracted many researcher' interest in the past few decades due to its inherent safety and high thermodynamics efficiency. During the reactor operation, it's inevitable that the impurities, such as the fission products, moisture, even the oxygen ion dissolved from the structure materials would be accumulated in the molten salt thus leading to the performance degradation of the reactor. Therefore, the fuel processing is required to reduce the inventory of the waste to improve the neutron economy and control the corrosion in the reactors.

Electrochemical method is highly favored for removing the impurities in the molten salt due to its widely investigation. Mostly, the electrolyte of this electrochemical method is dominated by the molten fluoride salt LiF (46.5mol%) - NaF (11.5mol%) – KF (42.0mol%) or LiF (66.7mol%) - BeF_2(33.3mol%). During the electrochemical separation process, the metal cations are reduced to metal or form compound with the cathode electrode if electrode is active enough to react with the metal. Meanwhile, the anions in the electrolyte could be oxidized to produce gas which will spread out the electrolyte thus realizing the goal of removing the anions from the molten salt. But there is also another concern that the gas may react with the component of the molten salt to introduce new impurity to the molten salt. Therefore, more attentions should be casted to choose appropriate electrodes.

The ideal electrode materials applied in the electrochemical experiment should be highly conductive and resistant to high temperature. Therefore, tungsten and graphite electrode have been widely used in the electrochemical process due to their low cost and high thermal stability. As for tungsten, in general, it is categorized as inert metal which is stable at high temperature, while for graphite, its gaseous products can be easily separated from the molten salt without much effort thus making it a good choice if the oxygen ions need to be removed in the solution. However, tungsten rod may dissolve when an appropriate potential was applied, which would contaminate the molten salt, also make the impurities, such as oxygen ions, removal impossible. When consumable carbon anodes are employed in molten fluoride salts, it was reported that some intermediate perfluorocarbon C_xF_y would be produced on the surface of anode electrode. These compounds with low surface energy often decompose slowly which leads to worse wettability of carbon anode, then result in more gas accumulation [19]. Finally, the thick layer of bubbles and solid perfluorocarbon would cover the anode surface, choking the passage of current and causing the cell voltage increasing. Such phenomenon is called “anode effect” which could lead to significant energy consumption and safety issues [20].

Until recently, there is still not enough studies on the electrochemical behavior of lanthanum oxide in fluoride melt. M. Ambrova [21] studied the electrochemical behavior of La_2O_3 in LiF-CaF_2 system and concluded that the electro-deposition of lanthanum on metal cathodes cannot be achieved in molten LiF or in LiF-CaF_2 without depolarization. But with active cathodes copper and nickel, a liquid alloy could be formed on the copper cathode, while intermetallic compounds LaNix was formed on the nickel cathode. In 2001, Stefanidak [17] studied the electrodeposition of neodymium in LiF-NdF_3, LiF-Nd_2O_3 and LiF-NdF_3-Nd_2O_3 melts. It was found that neodymium oxyfluoride was formed in the LiF melt. The electroreduction of neodymium

fluorides to neodymium metal in LiF-NdF_3-Nd_2O_3 on tungsten cathode was detected. During the oxidation of neodymium oxyfluoride, oxygen was evolved on the anode at less positive potential compared to fluorine evolution. There are also several studies on the electrochemical methods with graphite electrode which provide good references for the study. In 2003, Huan Qiao et al [22] proposed that the anodic products of oxygen ion at glassy carbon anode electrode at 3.0V (vs. K^+/K) were confirmed to be CO_2 and CO and the anodic process was proved to be an irreversible process. Later in 2010, Z. Huang's study [23] on the anode process of carbon electrode in LiF-NaF-KF melts demonstrated that the anode effect occurred at the potential higher than 3.7V (vs. K^+/K) and would produce perfluorocarbons, e. g. CF_4, C_2F_6, on the anode electrode.

To further understand the electrochemical behavior of La_2O_3 in the LiF-NaF-KF as well as the electrodes' effect on the electrolysis process, a detailed investigation was conducted in this study. Different electrodes were applied to verify if the lanthanum and oxygen elements can be separated from the molten salt.

3.2. Experimental Setup

LiF (BioUltra, ≥99.0%, Sigma), NaF (ACS regent, ≥99.0%, Sigma-Aldrich), KF (ACS regent, ≥99.0%, Sigma-Aldrich) and La_2O_3 (≥99.9%, Aldrich) were used in this experiment. Without special noting, all the operations are done in the glove box with < 1.7 ppm O_2 level and < 2.0ppm H_2O level. 1.0104g La_2O_3 was placed on the bottom of the Nickle crucible which served as the salt container first. After that, 14.5893g LiF, 5.8299g NaF, 29.5528g KF were mixed well before adding into the Nickle crucible which would lay on the top of the La_2O_3 to ensure the system reach equilibrium as soon as possible. Then, the possible impurities consisted in the

fluoride salts and hidden in the furnace parts were removed following the procedures in section 2.2. Finally, the temperature would be set at 700°C and keep heating for more than 48 hours before any measurements were carried out.

4 electrochemical experiments were designed to study the behavior of La_2O_3 in the molten salt with tungsten (≥99.5%, 3.2mm and 1.6mm) and graphite (99.999%, 3mm) electrodes. The single difference between these 4 experiments was the materials of the working electrodes and counter electrodes as shown in Table 3-1.

Three-electrode cell was utilized in the experiment at 700°C as shown in Figure 3-1. All voltammetric experiments were carried out in the furnace capable of sustaining a constant temperature. Insulation materials are used to keep a lower temperature gradient during the experiment operation. Quartz tubes were used for the isolation between electrodes and the stainless steel tubes. Electrodes bathed in the dilution water were cleaned in the ultrasonic machine for 40 minutes. In addition, all the electrodes were heated in the furnace for more than 24 hours before being inserted into the melt.

All the electrochemical experiments were performed with Gamry interface 1000 which was controlled by the Gamry Instruments Framework software. The transient electrochemical techniques, e.g. cyclic voltammetry (CV), chronopotentiometry (CP) and open circuit potential (OCP), were used to examine the electrochemical behavior on the working electrodes in the molten fluoride salt. In addition, without special noting, all the potential shown in the curves are relative to the tungsten reference electrode. X-ray powder diffraction analysis (XRD) was also done to identify the phase patterns on the surface of the working electrodes.

Table 3-1 Electrodes implied in the electrochemical experiments

	1st experiment	2nd experiment	3rd experiment	4th experiment
Working electrode	tungsten	tungsten	graphite	graphite
Counter electrode	tungsten	graphite	tungsten	graphite
Reference electrode	tungsten	tungsten	tungsten	tungsten

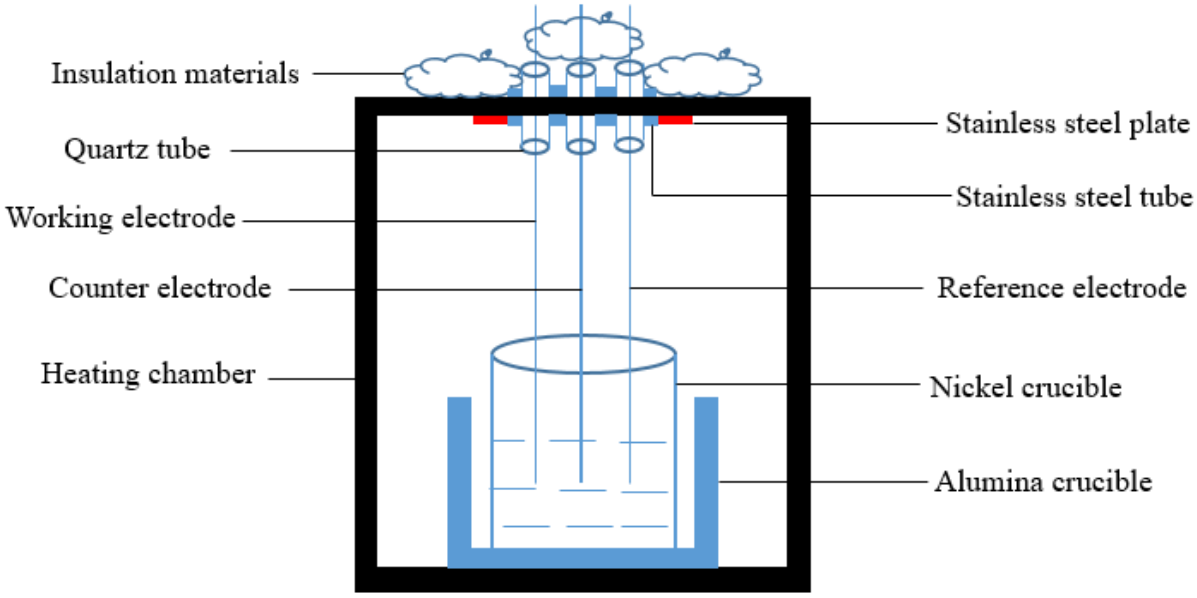

Figure 3-1 Electrochemical experimental setup sketch

3.3. Results and Analysis

3.3.1. 1st Experiment with Tungsten as Working, Counter and Reference Electrode

A typical curve of cyclic voltammetry from -1V to 0V of the tungsten working electrode in FLiNaK-La_2O_3 system is shown in Figure 3-2. Two pairs of peaks A/A' and B/B' are presented. According to the reduction potential of K^+/K, Na^+/Na and Li^+/Li vs. F_2/F^- at 700°C, it's known that the potential of K^+/K is less negative than the other two pairs [24]. Also, T. Yamamura et al. has demonstrated that reduction potential of La^{3+}/La is less negative than that of K^+/K [25]. Therefore, peak B/B' would correspond to K^+/K. As shown in Figure 3-2, a cathodic peak A at -0.44V and the corresponding anodic peak A' were observed. Since it's not known if the reaction is reversible or irreversible, the number of the electrons involved in the anodic peak was calculated from the difference of the potential giving peak current E_p and the potential giving the half of the peak current $E_{p/2}$ based on equations given by,

$$reversible: \left|E_p - E_{\frac{p}{2}}\right| = 0.774\frac{RT}{nF} \quad (19)$$

$$irreversible: \left|E_p - E_{\frac{p}{2}}\right| = 1.857\frac{RT}{\alpha nF} \quad (20)$$

Where, $\alpha = 0.5$ [26].

For peak A, the calculated electrons number is 3.09 for reversible reaction and 14.83 for irreversible reaction, which is the evaluated electrons number transferred in this reactions. Moreover, the electrode reaction for the reduction of La^{3+} can be expressed by,

$$La^{3+} + 3e^- = La \quad (21)$$

Which matches well with the transferred electron number 3.09, therefore, the peak A/A' in Figure 3-2 corresponds to the reaction of La^{3+}/La.

Since tungsten serves as working electrode in this experiment and La_2O_3 exists in the molten fluoride salt, the following reactions of the Gibbs free energy formation are calculated by,

$$W + O_2 = WO_2, \qquad \Delta G = -412.342kJ \tag{22}$$

$$W + \frac{3}{2}O_2 = WO_3, \qquad \Delta G = -592.298kJ \tag{23}$$

$$W + 2F_2 = WF_4, \qquad \Delta G = -970.030kJ \tag{24}$$

The Gibbs free energy of formation in these three reactions are less than 0, which indicates that once tungsten rod was exposed to O_2 or F_2 it's possible that the tungsten oxide and tungsten fluoride would be produced. Since the Gibbs free energy of reaction in *(24)* is more negative than the other two reactions, therefore, in the electrochemical experiment, it is assumed that the following reaction would dominate the anodic reaction under positive potential, which is given by,

$$W + 4F^- - 4e^- = WF_4 \tag{25}$$

As shown in Figure 3-3, the scan potential of the cyclic voltammetry is from 0.2V to 1.5V, the curve is characterized by the strong fluctuation. If the scan maximum potential limit is increased from 1.5V to 2V and 2.2V as shown in Figure 3-4 and Figure 3-5, the corresponding maximum current will quickly increase from 0.33A to 0.79A and 1.00A (the maximum current loaded in Gamry). Since the assumption that tungsten could combine with fluorine ions to produce the tungsten fluoride was proposed, it's possible that the fluorine gas production would adhere on

the surface of the working electrode before reacting with tungsten rod thus resulting in the passivation on the surface of working electrode which lead to the fluctuation in the curve. Since tungsten fluoride is soluble in the molten fluoride salt, as long as the potential goes up more than 0.8V, the combination between tungsten and fluorine ions will keep taking place thus resulting in increasing current. Moreover, after the electrochemical experiment, it was found that the diameter of the tungsten working electrode was about 0.815 mm less than that before the experiment which further confirmed that tungsten could react with fluoride ions to produce tungsten fluoride thus leading to its dissolving.

Shown in Figure 3-3, Figure 3-4 and Figure 3-5, it's obvious that all the cyclic voltammetry curves coincide with the assumption, the fluctuation peaks observed in the curve represent the production of tungsten fluoride.

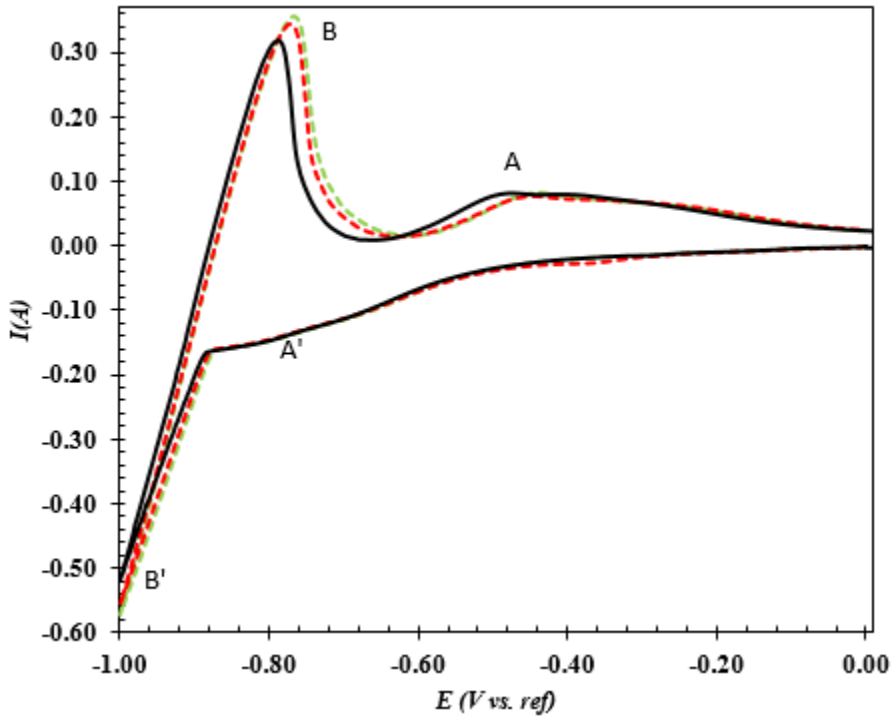

Figure 3-2 cyclic voltammetry, scan rate: 100 mv/s, working electrode: tungsten, counter electrode: tungsten, reference electrode: tungsten

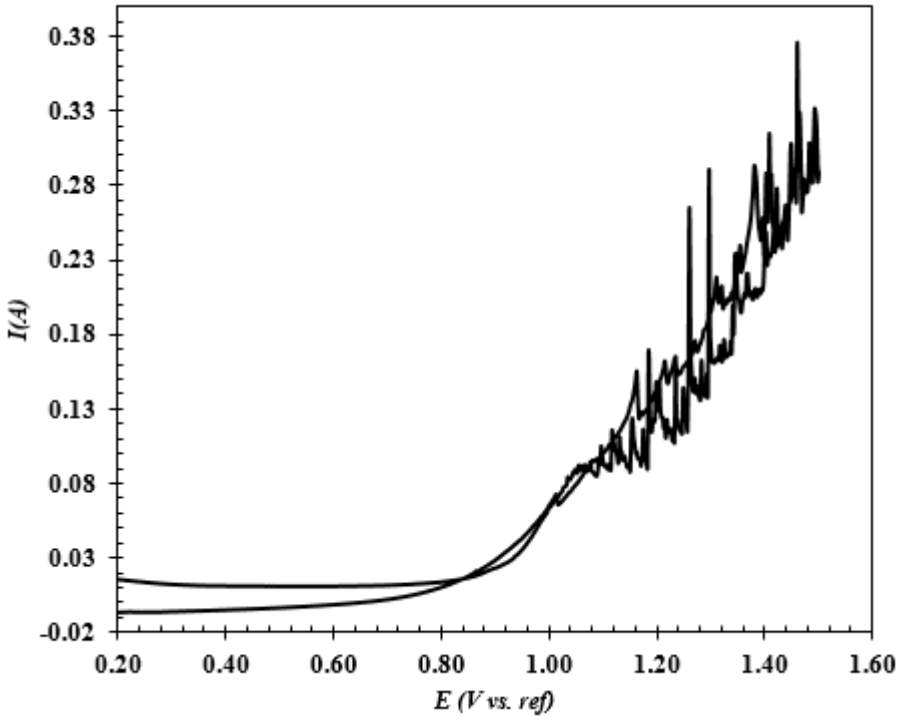

Figure 3-3 cyclic voltammetry, scan rate: 100 mv/s, working electrode: tungsten, counter electrode: tungsten, reference electrode: tungsten

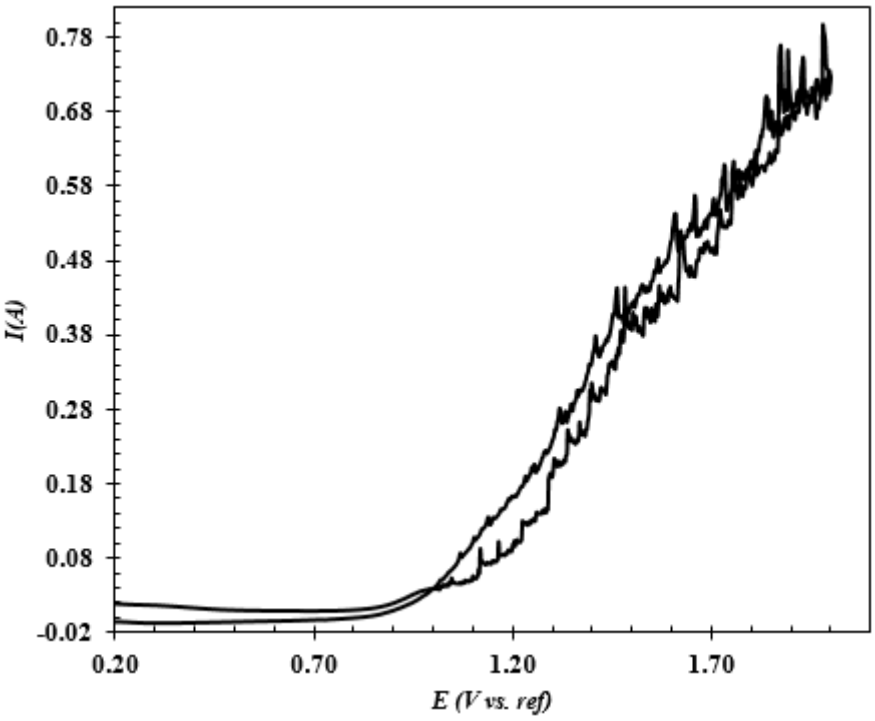

Figure 3-4 cyclic voltammetry, scan rate: 100 mv/s, working electrode: tungsten, counter electrode: tungsten, reference electrode: tungsten

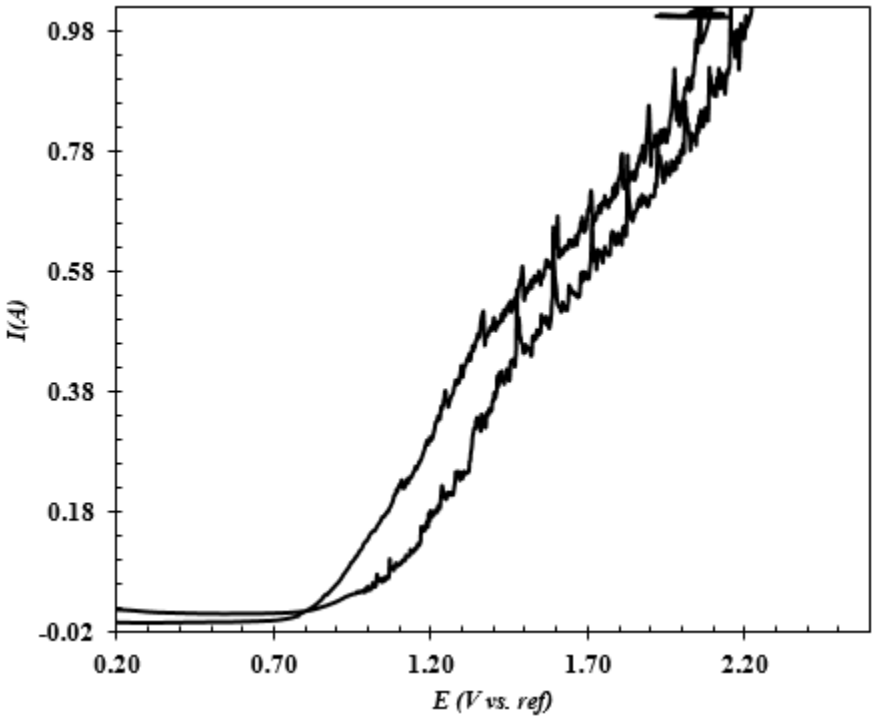

Figure 3-5 cyclic voltammetry, scan rate: 100 mv/s, working electrode: tungsten, counter electrode: tungsten, reference electrode: tungsten

3.3.2. 2nd Experiment with Tungsten as Working, Reference Electrode and graphite as counter electrode

Based on 1st experiment, it has been confirmed that tungsten rod could combine with fluorine ions to form tungsten fluoride during the anodic reaction process. Since tungsten serves as counter electrode in the 1st experiment, it has not been clear that whether the counter electrode materials could affect the electrochemical analysis result if that corresponding counter electrode has the possibility to react with some ions in the melt. Therefore, the 2nd experiment with graphite as counter electrode was designed the confirm the assumption.

In 2nd experiment, the experiment setup was kept as same as the 1st experiment except that the counter electrode was changed from tungsten to graphite. The obtained cyclic voltammetry curve with 100mv/s scan rate is shown in Figure 3-6. Comparing with the curve in Figure 3-2, these two cyclic voltammetry curves share the same trend and characteristics, both of which has two cathodic peaks and anodic peaks located at the same potential as shown in Figure 3-7. The only difference is that the peak current at B with tungsten counter electrode is about 0.2A larger than that with graphite counter electrode, which may result from the working electrode surface area immersed into the melt (surface area in 1st experiment was 50.27mm^2, while the surface area in 2nd experiment was 80.43mm^2) and the different internal resistance of the tungsten and graphite rod. Therefore, same to the analysis in 1st experiment, the B/B' corresponds to the reaction of K^+/K, while the peak A/A' represents the redox reaction of La in the melt. The different counter material's effect on the separation of lanthanum can be neglected except the peak current in the reaction of potassium which is possibly related to that.

As shown in Figure 3-8, the scan potential was set from -1.0V to 1.5V, the black curve is the cyclic voltammetry with graphite as counter electrode, while the red curve represents that with tungsten counter electrode. As expected, when the potential arrives in the range more than 0.8V, the current in the black curve begins to increase, then appears unstable fluctuation just as the same trend shown in the red curve due to the fluorine gas formation on the working electrode as discussed before. Therefore, it can be concluded that with different counter electrode, e. g., tungsten or graphite, both methods demonstrated the possibility of the lanthanum separation, while fluorine ions would react with tungsten in the anodic reaction to produce tungsten fluoride. Also, based on results of 1st and 2nd experiment, there is no significant evidence to confirm that

the counter materials applied in the experiment (tungsten and graphite) could affect the separation of lanthanum. Both works well in the FLiNaK-La_2O_3 melt system.

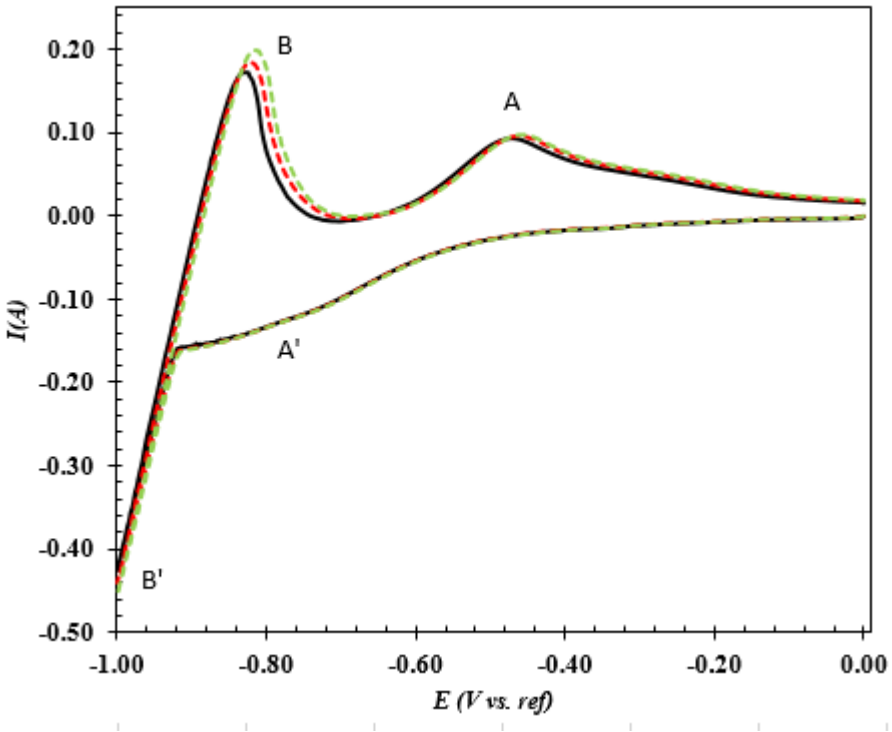

Figure 3-6 cyclic voltammetry, scan rate: 100 mv/s, working electrode: tungsten, counter electrode: graphite, reference electrode: tungsten

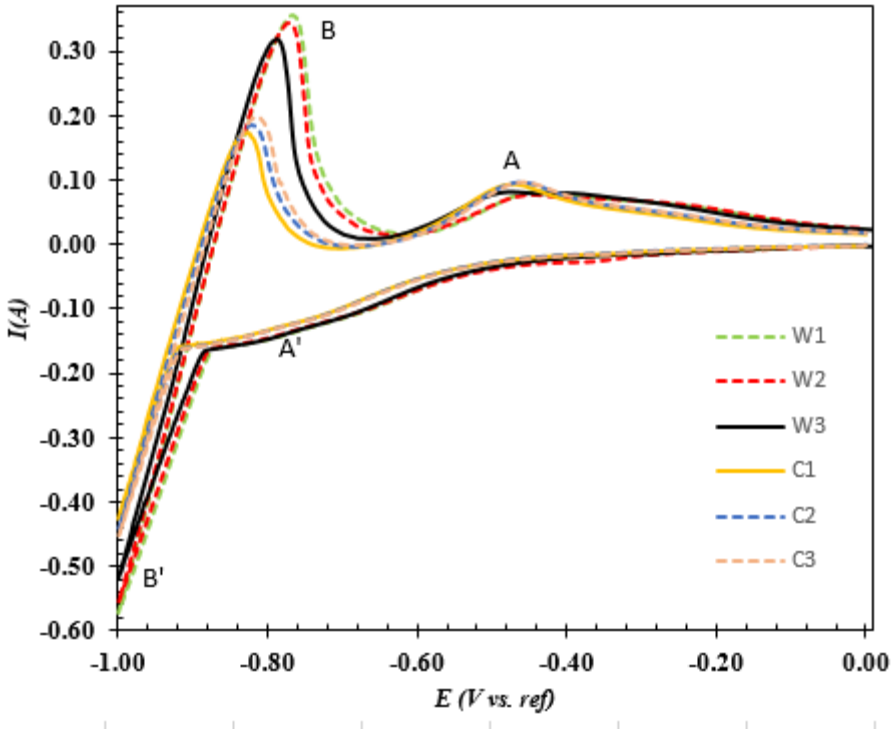

Figure 3-7 cyclic voltammetry, scan rate: 100 mv/s, working electrode: tungsten, counter electrode: tungsten (W1, W2, W3) and graphite (C1, C2, C3), reference electrode: tungsten. Surface area of tungsten: 80.43mm^2, surface area of graphite: 50.27mm^2

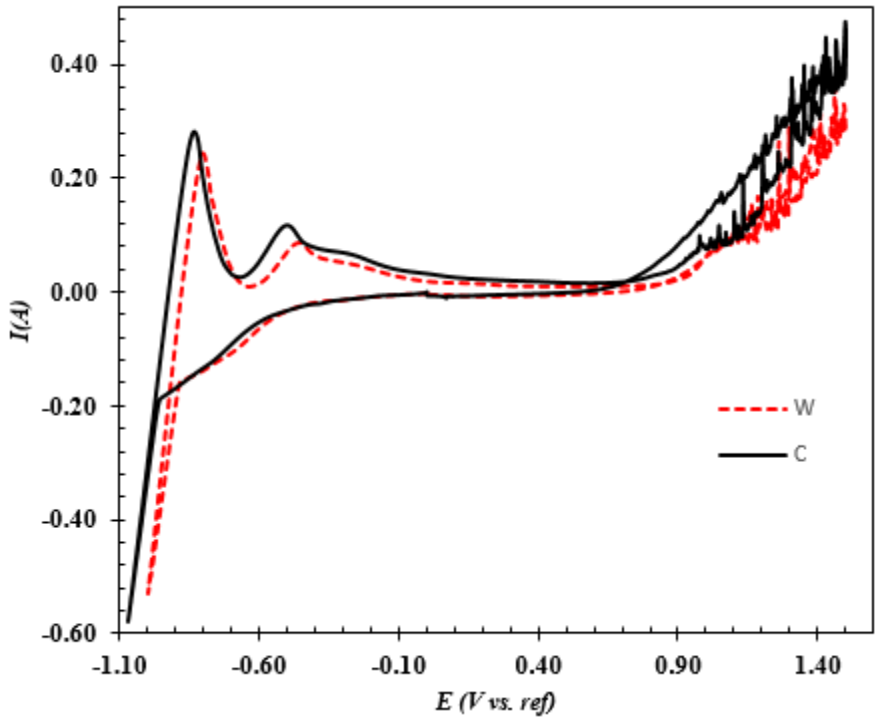

Figure 3-8 cyclic voltammetry, scan rate: 100 mv/s, working electrode: tungsten, counter electrode: graphite (C) and tungsten (W), reference electrode: tungsten

3.3.3. 3rd Experiment with Graphite as Working Electrode, Tungsten as Counter Electrode and Reference Electrode

In this experiment, pure graphite rod was applied instead of tungsten to serve as working electrode. As discussed before, the graphite rod plays the role of the sacrificial electrode which is expected to react with the oxygen ions in the melt to remove the impurities which has been studied in [20], [22] and [23]. When the potential was set from 0V to -3.2V, the cyclic voltammetry with different scan rates were obtained as shown in Figure 3-9. Comparing with the curves in Figure 3-2, Figure 3-6, Figure 3-7 and Figure 3-8, there is only one reduction peak when the potential scans from positive to negative direction with graphite working electrode. Moreover, the reduction potential vs. W at peak B' is much less negtive than that with tungsten

as working electrode. Considering that two oxidation peaks appeared in the curve, it was assumed that the reduction peak corresponding to peak A may be immersed into the peak B', in other words, the potential of corresponding reduction peak at A is close to the reduction peak at B, which lead to the absence of the reduction peak.

Another cyclic voltammetry experiment with pure FLiNaK was conducted to confirm the asumption. As shown in Figure 3-10, the black dash line represents the cyclic voltammetry result without La_2O_3. In the cyclic voltammetry curve of pure FLiNaK, the peak at C/C' correspond to the K^+/K due to its less negative potential than Na^+/Na and Li^+/Li. The potential at oxidation peak B is the same as K^+/K, which indicates that the peak B corresponds to the oxidation reaction of K^+/K. As for the peak A, the Gibbs free energy and the potential of the following reactions were calculated before further analysis which are given by,

$$\Delta G = -nEF \tag{26}$$

$$6KF + 1.5C + La_2O_3 = 2LaF_3 + 1.5CO_2 + 6K, \tag{27}$$

$$\Delta G_1 = 819.444kJ$$

$$\Delta E_1\ vs.\ O^{2-}/CO_2 = -1.4155V$$

$$La_2O_3 + 5.5C = 1.5CO_2 + 2LaC_2, \tag{28}$$

$$\Delta G_2 = 713.745kJ$$

$$\Delta E_2\ vs.\ O^{2-}/CO_2 = -1.2329V$$

$$La_2O_3 + 1.5C = 1.5CO_2 + 2La, \tag{29}$$

$$\Delta G_3 = 220.637kJ$$

$$\Delta E_3\ vs.\ O^{2-}/CO_2 = -0.3811V$$

$$La + 2C = LaC_2, \quad (30)$$

$$\Delta G_4 = -104.694kJ$$

The potential difference vs. O^{2-}/CO_2 in reactions between *(27)* and *(28)* is 0.1826V, while the difference between *(27)* and *(29)* is 1.0344V. Based on the calculated potential difference, if peak A was the oxidation of La, the difference between peak B and A should be close to theoretical value 1.0344, however, in Figure 3-9, the potential difference between these two peaks are about 0.15V, which is far less than 1.0344V, but can match the potential difference value between *(27)* and *(28)*. To further confirm the reaction at peak A, the electron transferred number is calculated with equation *(19), (20)*. Since both LaC_2 and La metal is hardly soluble in the molten salt and it is not known if the reaction is reversible or irreversible, after ohmic drop is corrected, the number of electrons involved in the electrode reactions is estimated to be 1.44 for reversible reaction and 6.91 for irreversible reaction. The estimated electron transferred number 1.44 is smaller than, but close to 1.5. Therefore, the reaction at peak A should correspond to C/LaC_2, not La/La^{3+}. In addition, since the peak B represents the oxidation reaction of K^+/K, it is surely that the corresponding reduction is included in peak B'. There are two evidence can support this assumption. First, potential difference vs. O^{2-}/CO_2 in *(27)* and *(28)* is very small which is only 0.1826V and the Gibbs free energy of *(28)* is smaller than *(27)* that would made the production of LaC_2 easier than deposition of K. Therefore, when the applied potential scans from positive to negative, at the beginning, La^{3+} will be reduced to La metal at the graphite rod surface then immediately react with C to form LaC_2, since the lanthanum carbide LaC_2 is a metallic conductor and hardly dissolve in the molten fluoride salt, it will adhere on the surface of the working electrode. Thus, the interface property will be changed due to the deposition of

LaC_2. As shown in Figure 3-10, the slope of B' is larger than that of C', which demonstrates the possibility that the reaction rate has increased after the interface property change. As a result, the formation of LaC_2 would make the over-potential of K reduction lower which shown in Figure 3-10 is that the reduction potential of K^+/K (-0.3V) in FLiNaK-La_2O_3 becomes much less negative than the "real" reduction potential of K^+/K (-0.85V) in the pure FLiNaK without La_2O_3. Another assumption is that the potential shift of K^+/K is due to the reference electrode potential shift in the electrochemical experiments. To verify this assumption, open circuit potential (OCP) measured before each cyclic voltammetry is shown in Figure 3-11. It's found that the potential shift between different experiments is less than 0.01V (much less than 0.15V), which further confirms the assumption that the production of LaC_2 is the main cause of the peak overlap shown in Figure 3-9.

Meanwhile, the dependence of the peak current on the square root of scan rates was plotted as shown in Figure 3-12 and exhibited good linearity, indicating that the oxidation reaction of LaC_2 was controlled by diffusion.

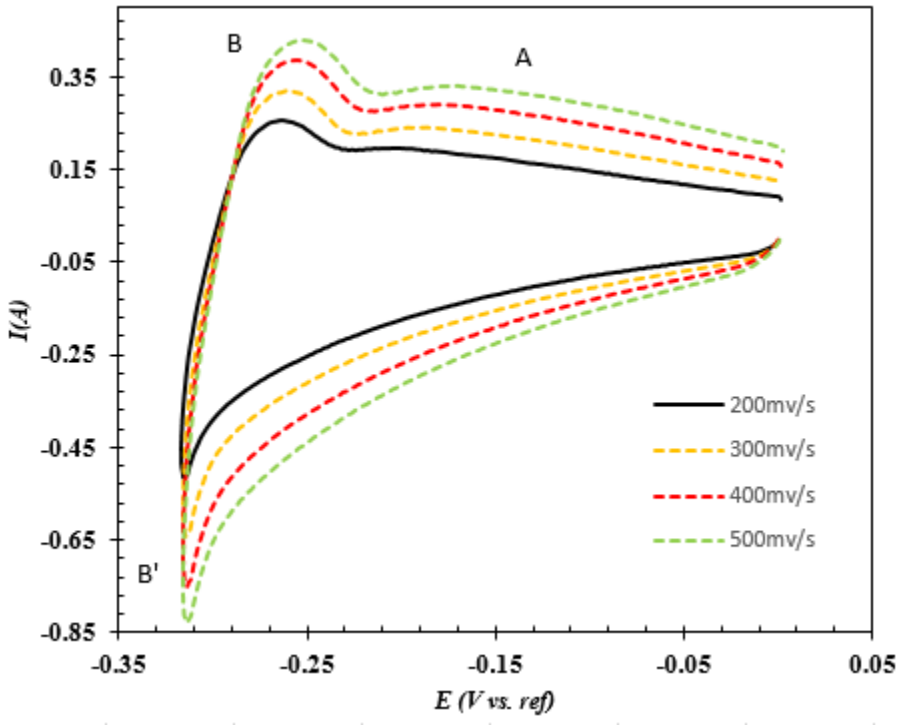

Figure 3-9 cyclic voltammetry, working electrode: graphite, counter electrode: tungsten, reference electrode: tungsten

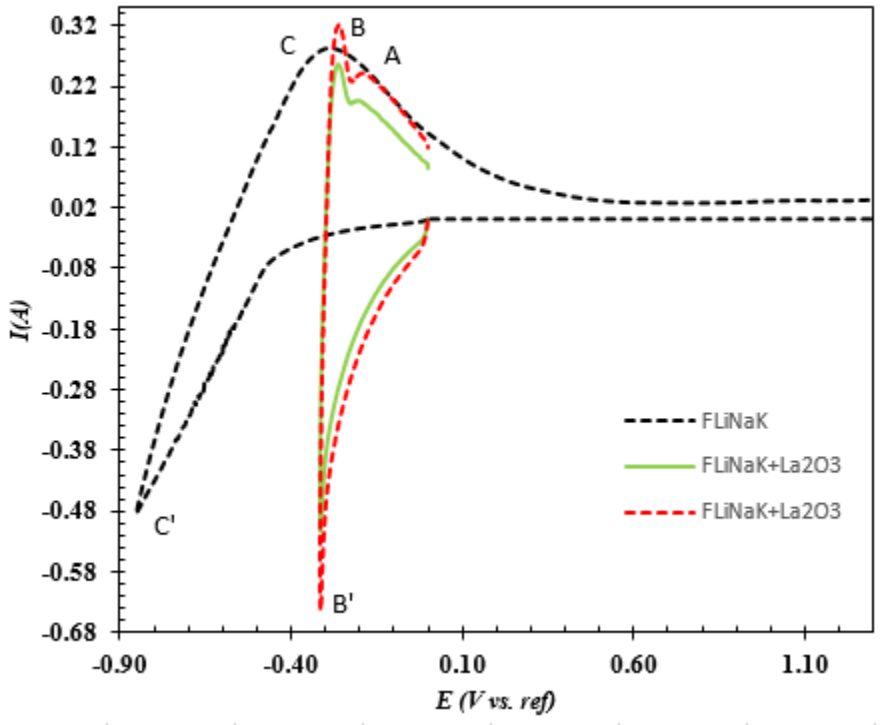

Figure 3-10 cyclic voltammetry, working electrode: graphite, counter electrode: tungsten, reference electrode: tungsten, red curve is FLiNaK without La_2O_3, green and red curve are FLiNaK with La_2O_3. Electrode surface area in pure FLiNaK: 89.54mm^2, electrode surface area in FLiNaK-La_2O_3 is 87.65mm^2.

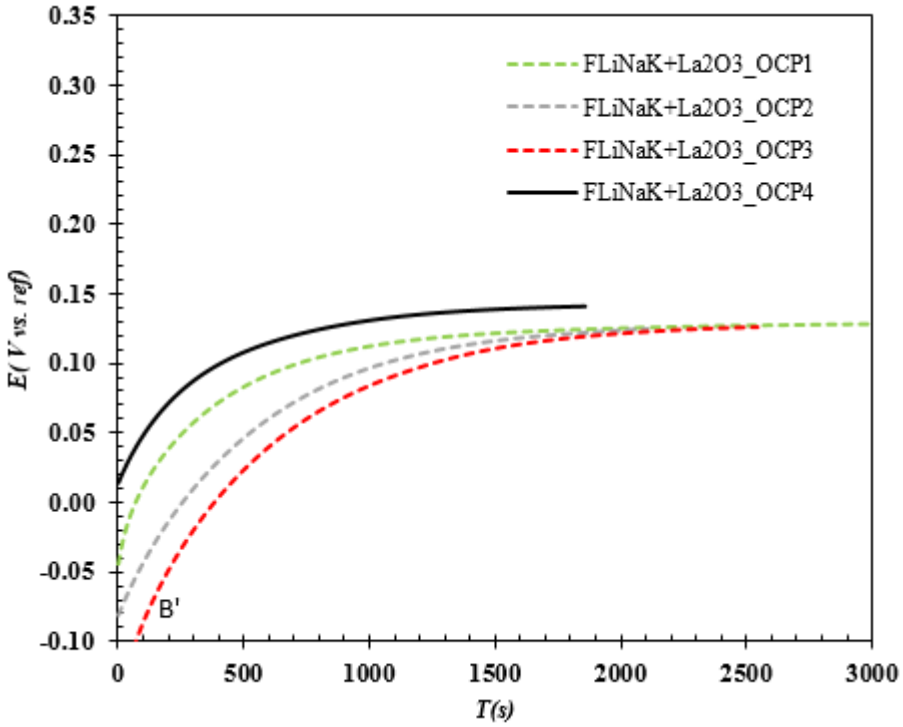

Figure 3-11 Open circuit potential at different time in the electrochemical experiment with working electrode: graphite, counter electrode: tungsten, reference electrode: tungsten

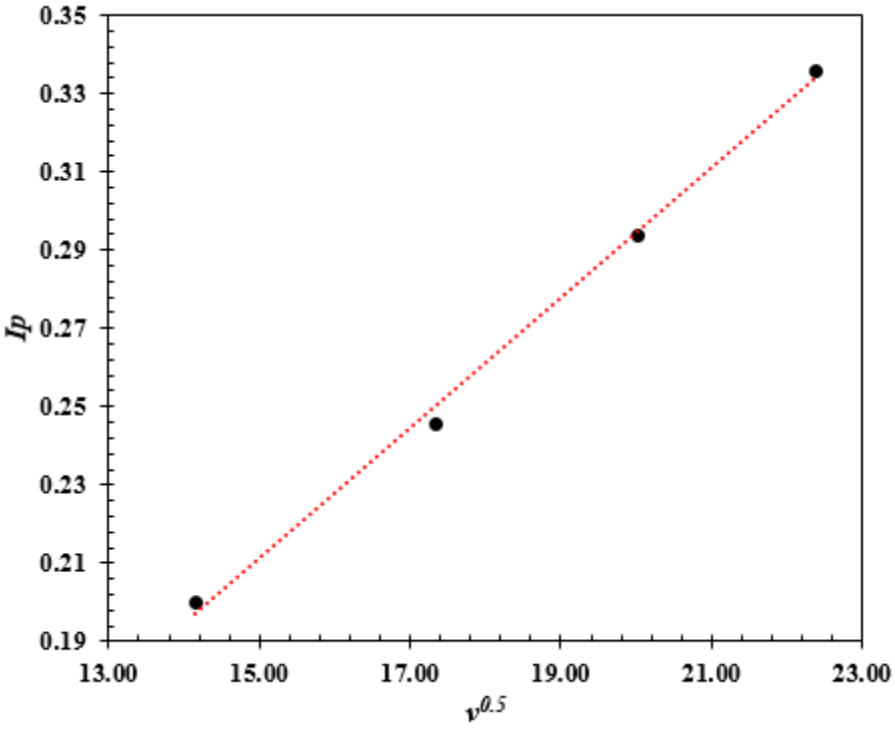

Figure 3-12 the dependence between the peak current and the square root of scan rate

When the cyclic voltammetry potential was scanned from 0V to more positive in the experiment, theoretically, the major contribution to anodic reactions should come from the dominant fluorine ions due to its large amount in the molten fluoride salt. Oxygen ions could also be involved for its less positive oxidation potential than fluorine ions. Therefore, the most possible reactions on graphite anode are given by,

$$C + O^{2-} - 2e^{-} \rightarrow CO \quad (31)$$

$$C + O^{2-} - 4e^{-} \rightarrow CO_2 \quad (32)$$

$$C + 4F^{-} - 4e^{-} \rightarrow CF_4 \quad (33)$$

$$2C + 6F^{-} - 6e^{-} \rightarrow C_2F_6 \quad (34)$$

$$2F^- - 2e^- \rightarrow F_2 \qquad (35)$$

As shown in Figure 3-13, the applied potential is scanned from 0V to 2.8V, an anodic peak was observed around 2.1V in region C. Since the similar result has been reported by Y. Ito and T. Yamamura [25] [27], this anodic peak should be contributed by the oxidation of oxygen ions with production of CO/CO_2. After the anodic peak, the stagnation of current was observed. In Figure 3-13, the region D with potential great than 2.3V would correspond to the production of C_xF_y due to the discharge of fluorine ions based on the study of [23] [28]. The whole reaction process dominating in region C and D can be described as: when the applied potential scans from 0V to 2.8V, at the beginning, the oxygen ions would discharge and react with graphite to form CO/CO_2 as shown in *(31)* and *(32)*, the bubbles could accumulate on the electrode surface thus decreasing the contact chance between the graphite and oxygen ions, which would lead to the current decreasing slowly until the oxygen ions around were consumed completely. As the applied potential keeps increasing, after it crosses the threshold value which is about 2.3V in this study to enter the region D, the main reaction would be the reaction between graphite and fluorine ions in the melt. The production in this region is much more complicated, e.g., CF_4 gas, C_2F_6 gas, and CF_x film et al. In Figure 3-13, it's found that the current goes down after about 2.5V until almost 0A before the reverse scan. This phenomenon is due to the formation of CF_x film on the graphite anode electrode. Once the reaction between graphite and fluorine ions begins, it would keep reacting much faster than graphite with oxygen ions until all the graphite surface immersed into the molten salt covered with the film. Then the passage between graphite and fluorine ions was cut off thus leading to the quick decreasing of current.

Moreover, if the applied potential was scanned from 0V until 6V as shown in Figure 3-14, the peaks related to the CO/CO_2 and C_xF_y in region C and D becomes more obvious than that in Figure 3-13. After the potential is greater than 2.7V, the current keeps at 0A without any fluctuation. The same phenomenon occurs even when the maximum potential was set at 10V as shown in Figure 3-15. This further confirms the formation of CF_x. Since more and more carbon fluoride was accumulated on the anode surface, finally, the whole surface contacting with the melt would be covered with the film which was nonconductive, thus the current in the cell becomes 0A. After that, no matter how the applied potential changes, since there is no more reactions between the graphite and fluorine ions, the current would be stable at 0A and reaction of *(35)* would impossibly happen which are shown in Figure 3-14 and Figure 3-15.

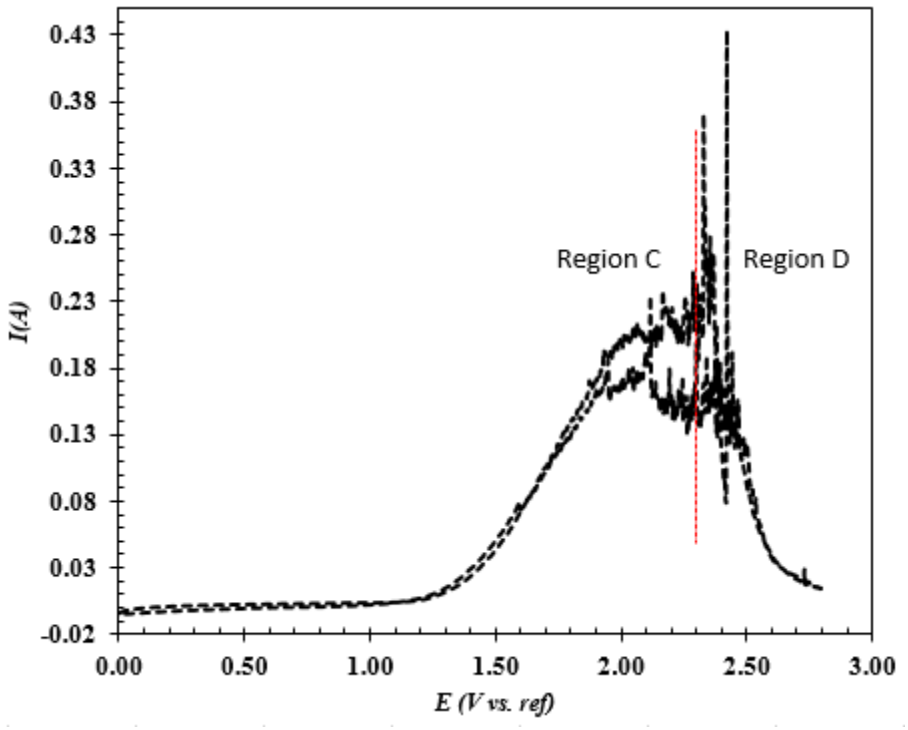

Figure 3-13 cyclic voltammetry, scan rate: 100 mv/s, working electrode: graphite, counter electrode: tungsten, reference electrode: tungsten

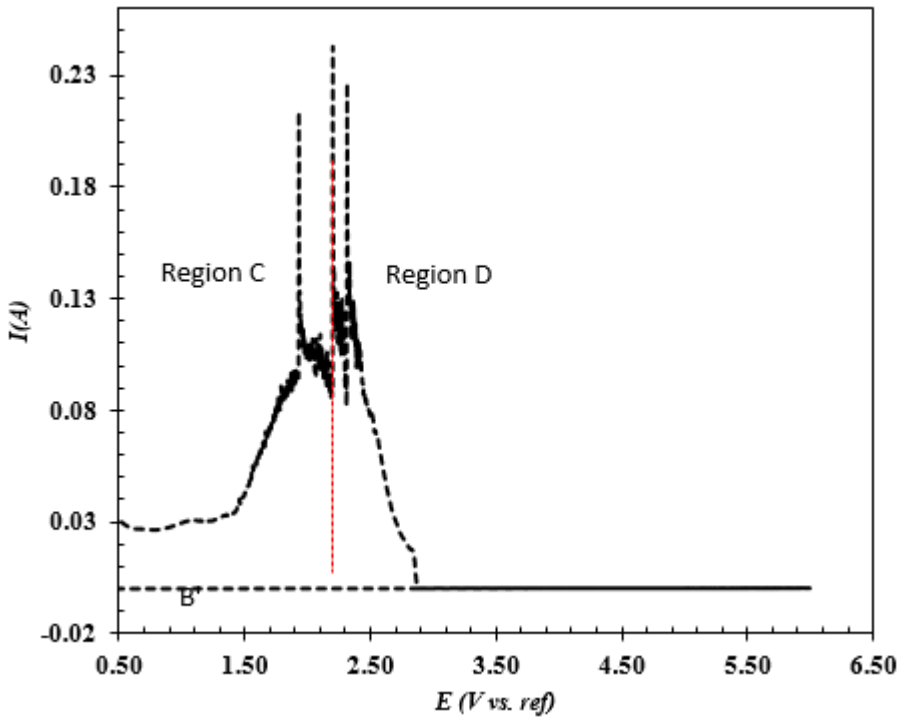

Figure 3-14 cyclic voltammetry, scan rate: 100 mv/s, working electrode: graphite, counter electrode: tungsten, reference electrode: tungsten

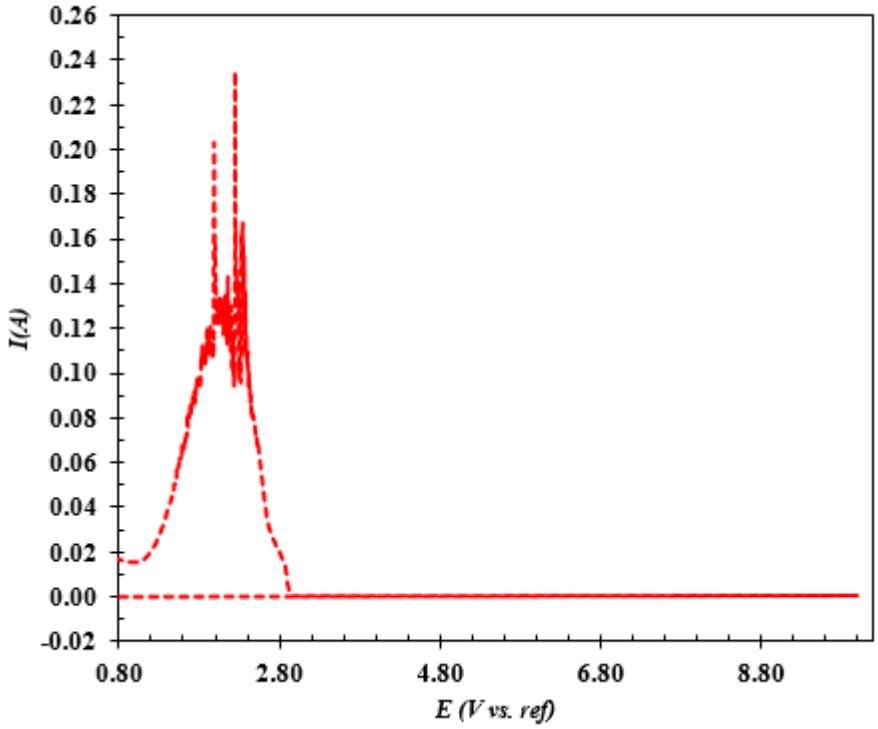

Figure 3-15 cyclic voltammetry, scan rate: 100 mv/s, working electrode: graphite, counter electrode: tungsten, reference electrode: tungsten

3.3.4. 4th Experiment with Graphite as Working Electrode and Counter Electrode, Tungsten as Reference Electrode

Another electrochemical experiment was also conducted with graphite as working electrode and counter electrode, tungsten as reference electrode. Typical cyclic voltammetry curves were obtained with scan rate 100mV/s, 200 mV/s, 300 mV/s and 400 mV/s in Figure 3-16. And the dependence of the peak current and the square root of scan rate also shows linear relationship in Figure 3-20 which demonstrates that the reaction at peak A is controlled by the diffusion in the melt. A cyclic voltammetry curve was also obtained with pure FLiNaK without La_2O_3 and the comparison between pure FLiNaK and FLiNaK-La_2O_3 curves are shown in Figure 3-17. Comparing the curves in Figure 3-16 and Figure 3-17 with those in Figure 3-9 and Figure 3-10, it

is obviously that the cyclic voltammetry curves share the same characteristics. In addition, the corresponding open circuit potential is also shown in Figure 3-18 which indicates the reference electrode potential shift is less than 0.01V, demonstrating that the reduction peak of La^{3+}/LaC_2 and peak K^+/K has overlapped in peak B' due to the production of LaC_2 as discussed before. Moreover, chronopotentiometry with constant currents of 9mA and 10mA were done to further verify the two reduction reactions overlapped in peak B'. As shown in Figure 3-19, two plateaus A and B present in the curves individually. According to the calculated Gibbs free energy in *(27)* and *(29)* and the corresponding potential at each plateau, plateau A at about 0.35V indicates that the reaction of La^{3+}/LaC_2 is undergoing, while plateau B at about 0.40V is the reflection of the reduction reaction of K^+/K which happens right following the reaction of La^{3+}/LaC_2.

In addition, since the Gibbs free energy of reaction *(27)* is greater than 0 kJ/mol, it is thermodynamically impossible that LaC_2 would be produced without external charge in the heating process. Therefore, the XRD samples were taken from the graphite working electrode surface after the chonopotentiometry scan with a constant current 10mA to identify the phase patterns. As shown in Figure 3-21, LaC_2 was found in the samples which further confirms that the reaction of La^{3+}/LaC_2 does happen in the electrochemical process and peak A in both of Figure 3-9 and Figure 3-16 represent the oxidation reaction of LaC_2.

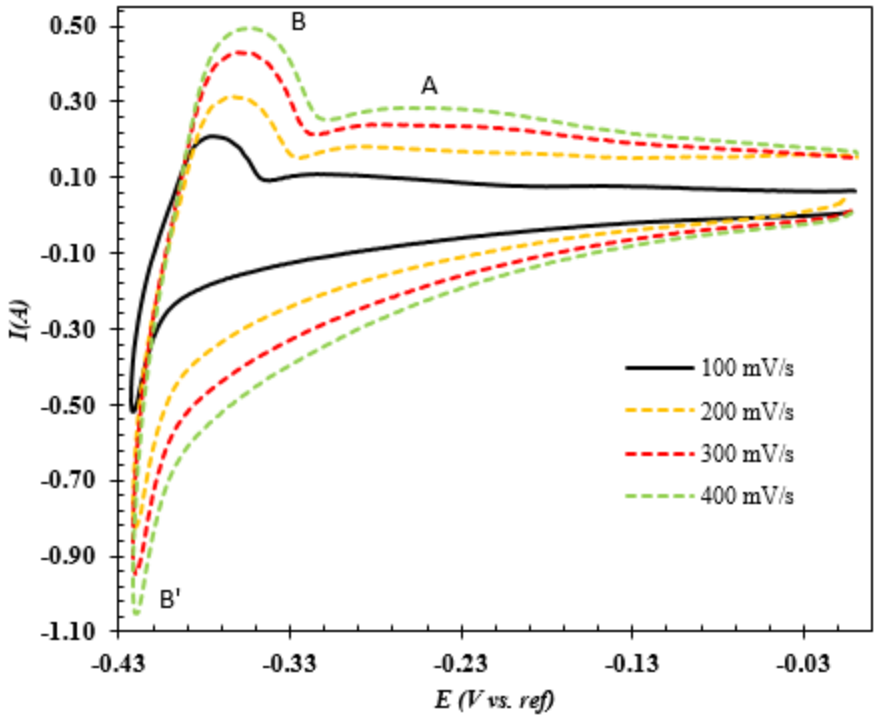

Figure 3-16 cyclic voltammetry, working electrode: graphite, counter electrode: graphite, reference electrode: tungsten

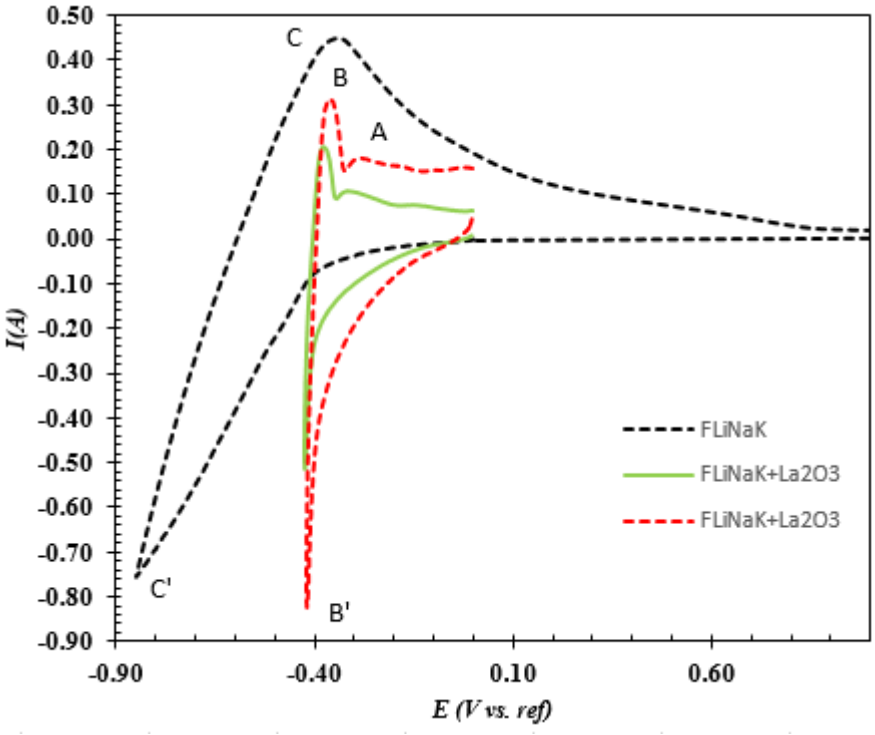

Figure 3-17 cyclic voltammetry, working electrode: graphite, counter electrode: graphite, reference electrode: tungsten. Electrode surface area in pure FLiNaK is 94.25mm^2, electrode surface area in FLiNaK-La_2O_3 is 44.88mm^2

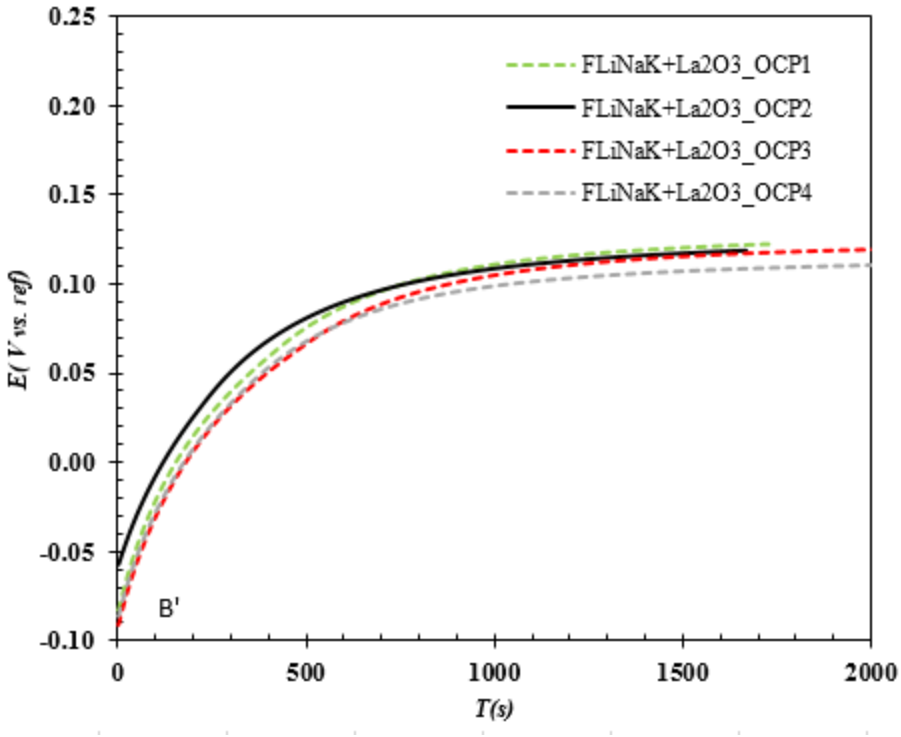

Figure 3-18 Open circuit potential at different time in the electrochemical experiment with working electrode: graphite, counter electrode: graphite, reference electrode: tungsten

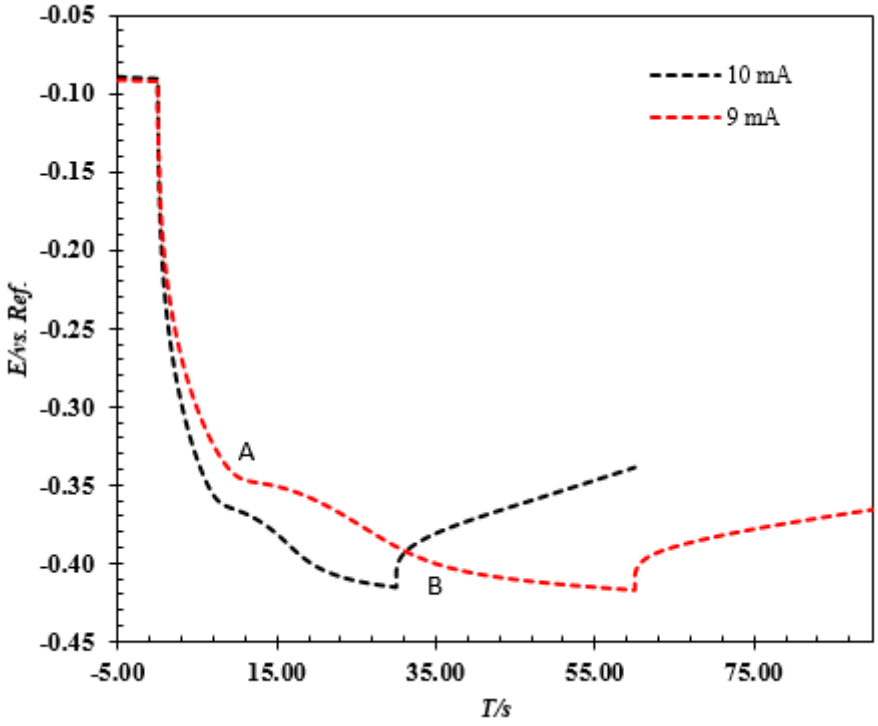

Figure 3-19 chronopotentiometry, working electrode: graphite, counter electrode: graphite, reference electrode: tungsten

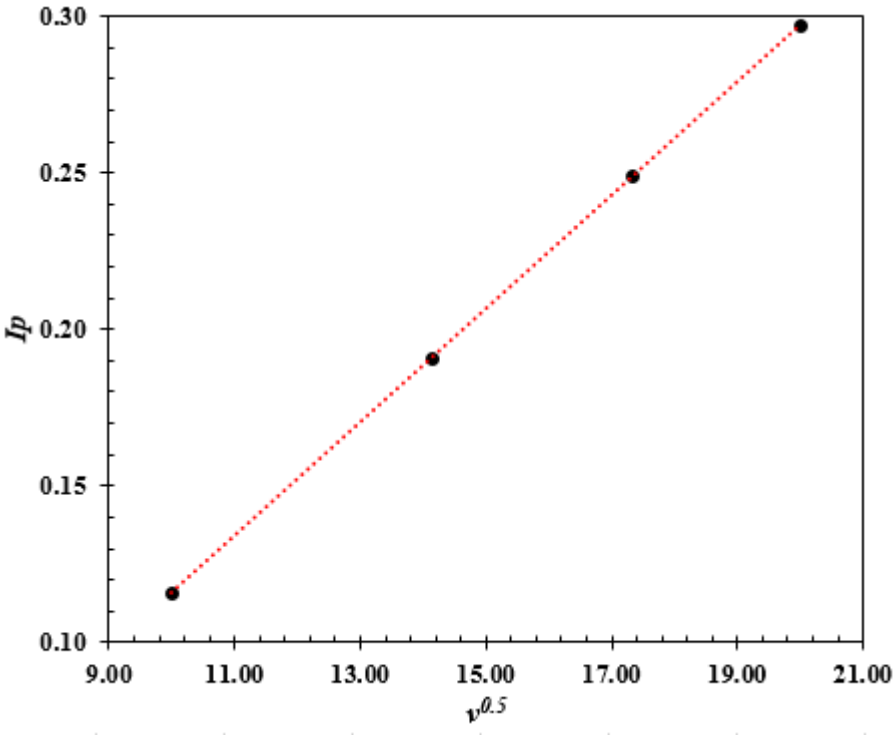

Figure 3-20 the dependence between the peak current and the square root of scan rate

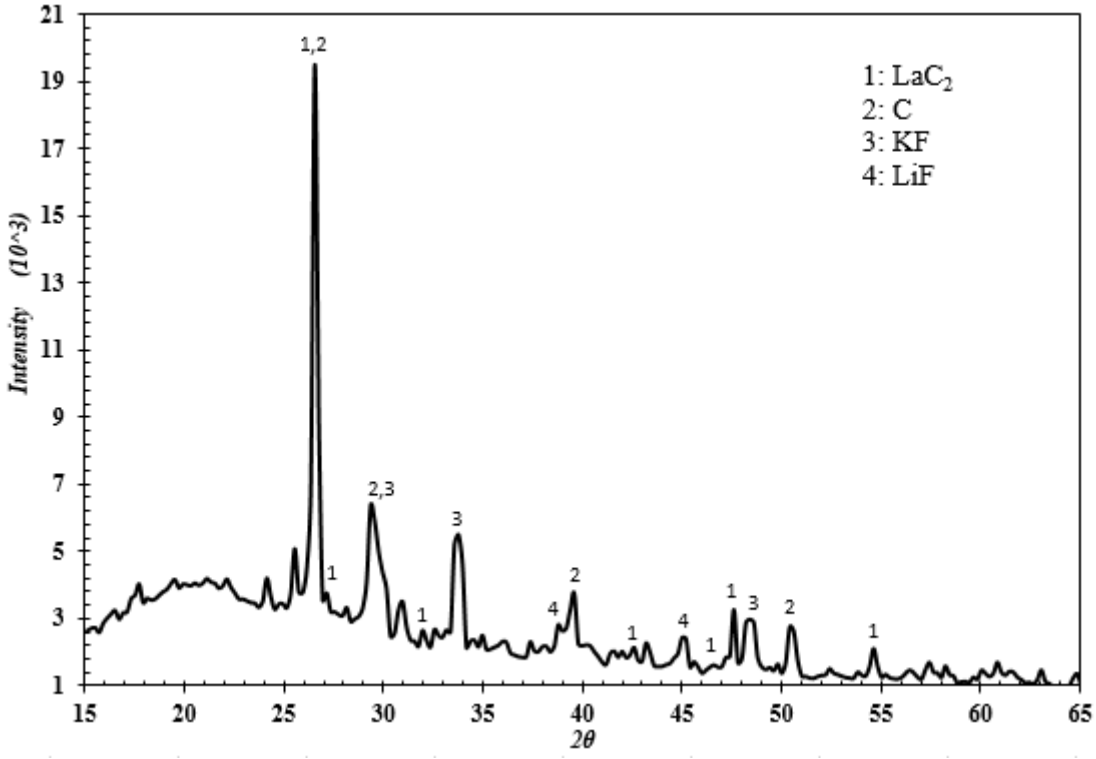

Figure 3-21 X-ray powder diffraction analysis on the graphite surface after deposition

When a positive potential was applied, the cyclic voltammetry curves were obtained as shown in Figure 3-22, Figure 3-23 and Figure 3-24. Comparing with the curves in the 3rd experiment, there is no significant difference. When the applied maximum potential is 1.68V shown in Figure 3-22 and Figure 3-23, the fluctuation in the curve is weak and the reverse scan current is almost the same at the higher potential which mean that the reaction is still in the region C and the reaction is related to the formation of the carbon oxide. Then the maximum scan potential was increased to 2.0V in Figure 3-23, which is just the peak potential of carbon oxide in 3rd experiment, it was observed that the fluctuation becomes more severe near 2.0V due to the large amount of carbon oxide bubbles on the electrode surface. Finally, when the maximum peak was set at 2.8V, another region D occurs as expected which is contributed by the reaction of graphite and the

fluoride ions. Meanwhile, the current at the reverse scan also becomes much smaller than before due to the anode effect on the electrode surface.

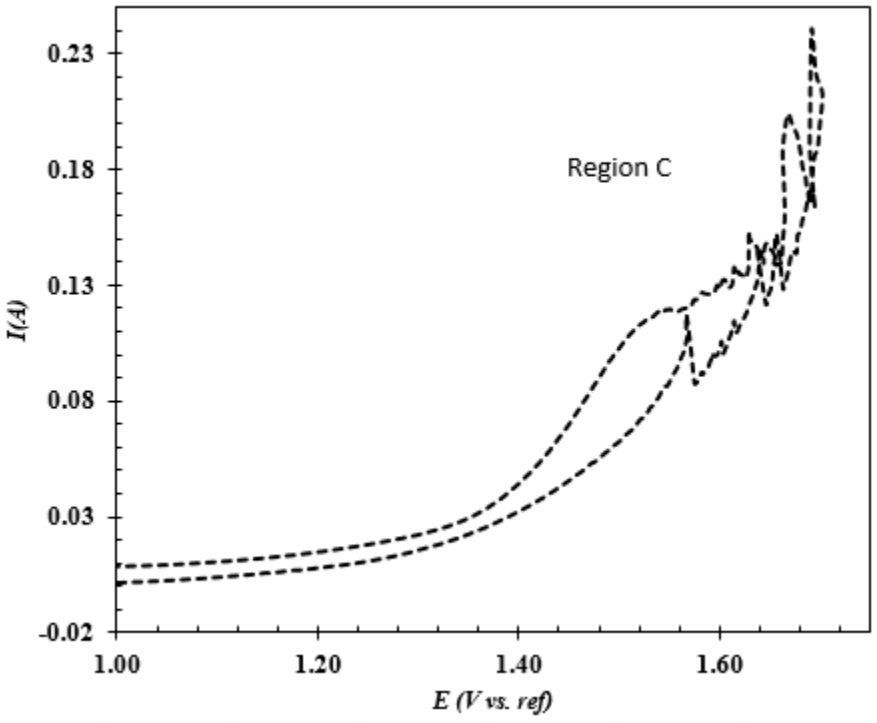

Figure 3-22 cyclic voltammetry, working electrode: graphite, counter electrode: graphite, reference electrode: tungsten

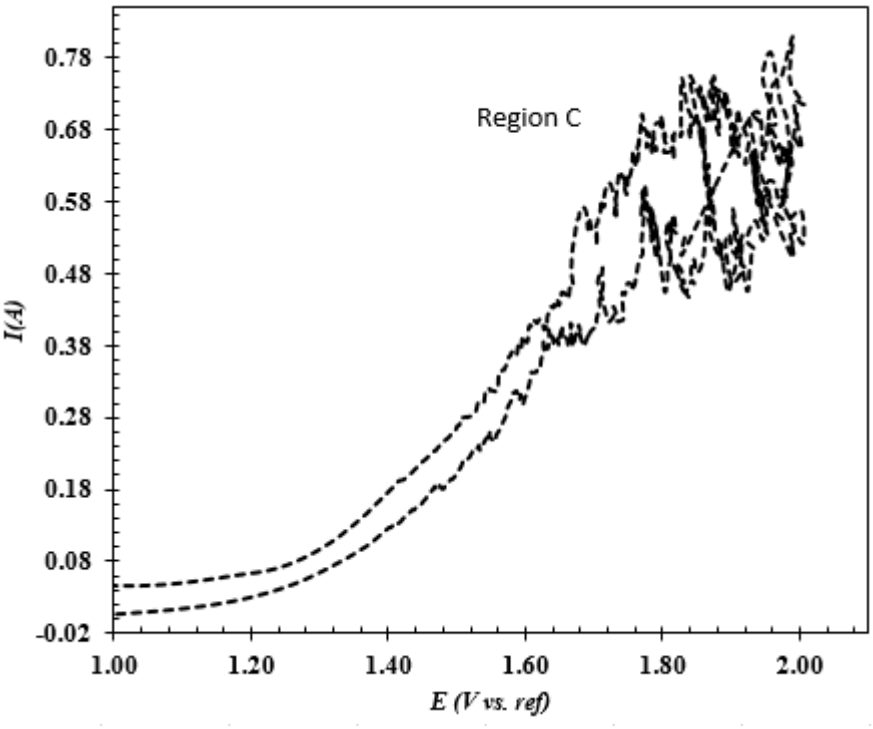

Figure 3-23 cyclic voltammetry, working electrode: graphite, counter electrode: graphite, reference electrode: tungsten

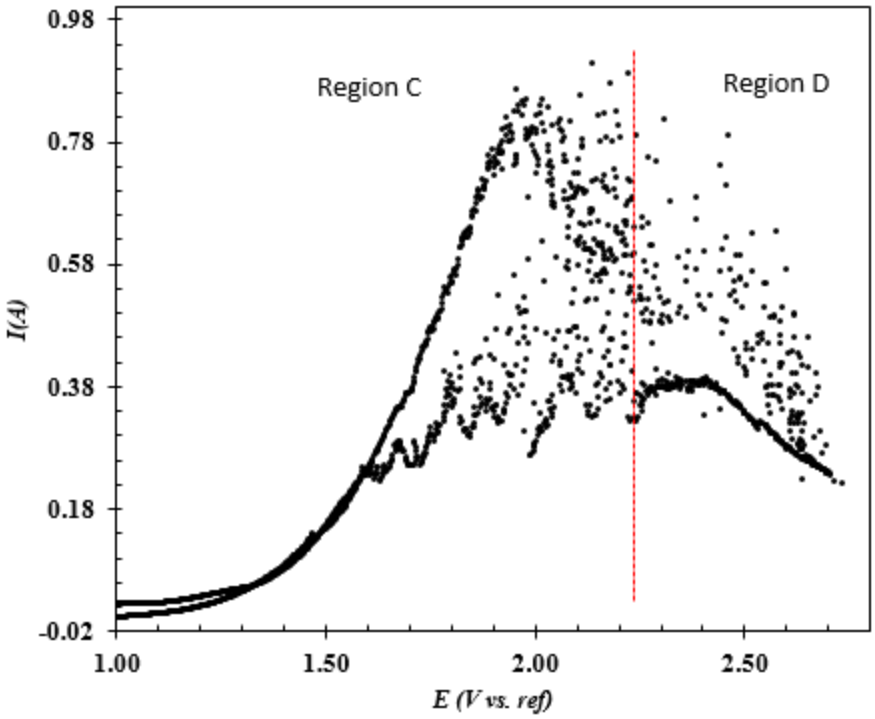

Figure 3-24 cyclic voltammetry, working electrode: graphite, counter electrode: graphite, reference electrode: tungsten

3.4. Conclusions and Future work

The electrochemical behavior of La_2O_3 in molten FLiNaK salt was investigated by cyclic voltammetry, chronopotentiometry and open circuit potential techniques at 700°C with tungsten or graphite as working or counter electrode. In this study, lanthanum ions can be reduced to lanthanum metal on the tungsten cathode electrode, while the fluorine ions would react with tungsten anode electrode to form tungsten fluoride, e.g. WF_4, thus leading to the dissolving of tungsten and introducing new impurity into the molten salt. Therefore, tungsten electrode is not a good choice when applied to oxygen ions removal. As for the graphite electrode, it performed well both for the lanthanum and oxygen element separation. With graphite working electrode, lanthanum ions could be reduced in the form of LaC_2, while oxygen ions would be oxidized to

CO/CO_2 which is easy to be separated from the solution with low cost. The only concern regarding to the graphite anode is the "anode effect" resulted from the CF_x film formed at higher potential. If applied in industry, the sever anode effect would lead to huge energy consuming thus increasing the impurities removal cost. Therefore, more work still need to be conducted in the future.

4. First Principle Molecular Dynamic Simulation Study of Molten FLiNaK and FLiNaK-La_2O_3 Salt

4.1. Introduction

Molten fluoride salt has been studied for a long time as a coolant or the fuel salt for the nuclear molten salt reactor due to its good performance as an effective heat transfer at high temperature and high radiation flux conditions. Oak Ridge National Laboratory (ORNL) has conducted a series of molten salt reactor experiment (MSRE) in 1960s to assess the potential application of molten fluoride salts for nuclear power plant. Moreover, fluoride-cooled high temperature reactor (FHR) was also proposed to use molten fluoride salt as the coolant. Although there have been extensive thermo-kinetic properties of molten salts obtained in MSRE program, more data are still needed from both of experiments and model to validate the existing experiment data and achieve new data about the molten salt properties. But experimental measurement on the molten salt is always time consuming and limited by the huge cost due to the harsh experiment conditions, e.g., high temperature. It is difficult to accurately acquire the basic physicochemical data about the molten salt mixture with experiments. While computation simulations provide a low cost alternative comparing with experiments and could explore many different temperatures and salt compositions.

In classical molecular dynamics, the force field model is used as the fundamental input thus any classical molecular dynamics simulation depends on the availability and the accuracy of the force field. In addition, classical interaction potentials molecular dynamics (IPMD) lose sight of the interaction between electrons and therefore doesn't work well to study the relevant electronic

property. The density function theory [29] based on the first principle molecular dynamics (FPMD) [30] is the most accurate route to build a predictive model for the whole system due to its realistically accounts for many-body effects like charge transfer and polarization. First principle molecular dynamics simulation calculates the interionic forces from first principles on the fly and thus avoid the empirical force field models. It has several advantages over the classical interatomic potential molecular dynamics, e. g. higher accuracy of full quantum mechanical calculation of the forces, the abilities of studying any systems without interatomic potential and obtaining the electronic properties which the IPMD cannot calculate. The main disadvantage of FPMD is that the calculations are very computationally intensive and therefore it has to be limited to smaller systems and shorter simulation times than IPMD.

Recently more and more molecular dynamics simulation tools have been developed, which, in the other hands, also helped to speed up the development and application of the FPMD. There are several softwares that are often implemented in FPMD, e. g., Vienne Ab-initio Simulation Package (VASP) [31] [32] [35], CPMD [33] and Cambridge serial total energy package (CASTEP) [34] [35]. In addition, due to the rapid development of the supercomputer performances, FPMD is now able to be practically applied in the simulations of liquid systems [36] [37] [38] [39]. More and more work has also been done with these tools to study the properties of the molten salt, liquid metal and many other materials. H.O. Nam et al [40] studied two types of molten fluoride salt, LiF-BeF_2 and LiF-NaF-KF with Cr, Cr^{2+} and Cr^{3+} ions. In his work, the thermo-kinetic properties of the fluoride salt, i.e., equilibrium volume, density, bulk modulus, coefficient of thermal expansion and self-coefficient, as well as the effect of Cr valence on diffusivity and local structure in the salt were calculated in detail which provided a good reference for the FPMD's application. Moreover, J. Dai et al [41] also applied FPMD in the

simulation of identified clusters in gas phase and salts in condensed phase, through which to have an insight on the structure and vibrational spectra of the local structures in LiF-BeF_2 molten salts. In 2017, J. Song et al [42] combined classical molecular dynamics and FPMD to evaluate the densities of molten salt mixtures in NVT ensemble [43] and local coordination structures in terms of radial distribution functions, and self-diffusion coefficients and ion conductivities from the mean square displacements based on Einstein relation. X. Lv et al performed FPMD simulations to studied the ionic structure and transport properties of LiF-NaF-AlF_3 [44] and Na_3AlF_6 [45] with CASTEP code in 2016 and 2018 respectively.

In this study, FPMD is employed directly to model the molten fluoride salt at high temperature. The FLiNaK system composed of 46.5 mol% LiF, 11.5 mol% NaF and 42 mol% KF would be studied to determine local ionic structure and enthalpy of formation at 700°C. Firstly, details of computational method to simulate the molten fluoride salt system by FPMD are proposed. Basic structure information of pure fluoride salts was calculated and compared with the results in literatures to validate the FPMD modeling of fluoride salts. Then La atoms and O atoms were added to obtain the corresponding structure of FLiNaK-La_2O_3 system. Finally, the enthalpy of formation in pure FLiNaK and FLiNaK-La_2O_3 system were calculated as well as Gibbs free energy of LaF_3 and LaOF.

4.2. Computational Methods

4.2.1. **First Principle Molecular Dynamics Method**

Before FPMD simulation, the initial configuration of ions for the molecular dynamics were prepares by packing the ions randomly in the simulation cubic box via Packmol package [46]. For the model of FLiNaK, based on the industry component, 46.5 mol% LiF, 11.5 mol% NaF

and 42 mol% KF, the model was comprised of 23 Li atoms, 6 Na atoms, 21 K atoms and 50 F atoms with total 100 atoms. The cubic simulation model box was built with density of $2 \times 10^3 kg/m^3$ according to experimental data and lattice constant 11.83 Å. The obtained initial configuration was then run in the VASP to reach equilibrium. The equilibrium simulation was done in a canonical ensemble with fixed particle number, volume and temperature (NVT) using the algorithm of Nose [47]. A conjugate-gradient algorithm was used to relax the ions into their instantaneous ground state [48]. PAW-PBE potentials were used to simulate F(s2p5), Li(s1p0), Na(s1p0) and K(p6s1). Within the parenthesis, the valence electrons for each pseudopotential was specified. The projector augmented wave (PAW) method and a plane wave basis set with energy cutoff of 400 eV and energy convergence of 10^{-4} which is enough in most cases due to the fact that the convergence speed is exponential in the simulation. A $2 \times 2 \times 2$ k-point mesh was applied with KSPACING equal to 0.5. Finally, the configuration obtained from the equilibrium procedure was used in the molecular dynamics simulations with $1 \times 1 \times 1$ k-point mesh and time step of 2fs. The FPMD simulation data was obtained after 30ps which would be used to obtain the electronic structures. After that, 2 La atoms and 3 O atoms were added to simulate FLiNaK-La_2O_3 system, thus obtaining the corresponding local ionic structure.

4.2.2. **Radial Distribution Function**

The radial distribution function analysis was conducted from the molecular dynamics trajectories to study the local structure surrounding a certain ion. In statistical mechanics, the radial distribution function $g(r)$ in a system of particles describes how density varies as a function of distance from a reference particle. It is the probability distribution for particles surrounding another particle which is given by,

$$g(r[i]) = \frac{n_{pair}[i]}{v[i]} \cdot \frac{V}{N_{pair}} \quad (36)$$

Where, $n_{pair}[i]$: the number of pairs in bin $(r_i, r_{i+1} = r_i + dr)$

$v[i]$: volume of bin

N_{pair}: number of pairs

V: volume of simulation cell

While the first shell coordination numbers (CNs) is the average coordination number for one atom around the reference atom [49]. It is estimated by numerical integration of radial distribution function within a cut-off radius which corresponds to the first peak interval in the RDF. By integrating equation *(36)*, the first shell coordination number is obtain given by,

$$N_{ij} = 4\pi\rho_j \int_0^{R_{cut-off}} r^2 g_{ij}(r)\, dr \quad (37)$$

Where, $g_{ij}(r)$: the RDF between atom i and atom j

ρ_j: the average number density of reference atom in the center.

4.2.3. **Enthalpy of Formation $\Delta \boldsymbol{H_{mix}}$**

Assuming that a multicomponent solution of LiF-NaF-KF are mixed well in homogeneous state at 700°C, 1mol of solution contains $X_{Li}mol$, $X_{Na}mol$, $X_K mol$ and $X_F mol$ of Li, Na, K and F ions ($X_{Li}mol\ LiF, X_{Na}mol\ NaF, X_K mol\ KF$) in the molten salt. There are two steps of mixing: first ($X_{Li}mol$ pure LiF, $X_{Na}mol$ pure NaF and $X_K mol$ KF are brought together, then pure LiF, NaF and KF are mixed evenly to make a homogeneous solution. After the first step, the Gibbs free energy of the system is given by,

$$G_1 = X_{Li}G_{LiF} + X_{Na}G_{NaF} + X_K G_{KF} \quad (38)$$

Where, G_1: Gibbs free energy after step 1

G_{LiF}: Gibbs free energy of pure LiF

G_{NaF}: Gibbs free energy of pure NaF

G_{KF}: Gibbs free energy of pure KF

After step 2 the free energy of the system is given by,

$$G_2 = G_1 + \Delta G_{mix} \quad (39)$$

$$\Delta G_{mix} = \Delta H_{mix} - T\Delta S_{mix} \quad (40)$$

$$\Delta H_{mix} = H_2 - H_1 \quad (41)$$

Where, ΔG_{mix} is the Gibbs free energy change due to the mixing

ΔH_{mix}: heat of formation of the molten salt solution

ΔS_{mix}: entropy of formation of the molten salt solution

For the heat of formation ΔH_{mix}, the quasi-chemical model is applied in which the heat of mixing only dependent on the bond energy between the adjacent atoms, indicating that the interatomic distances and bond energies are independent of composition. In the molten FLiNaK salt, 10 types of bonds are included, i.e., Li-F, Li-Li, Li-Na, Li-K, Na-F, Na-Na, Na-K, K-F, K-K and F-F. Then, the internal energy of the solution is given by,

$$E = B_{Li-F}E_{Li-F} + B_{Li-Li}E_{Li-Li} + B_{Li-Na}E_{Li-Na} \quad (42)$$
$$+ B_{Li-K}E_{Li-K} + B_{Na-F}E_{Na-F}$$
$$+ B_{Na-Na}E_{Na-Na} + B_{Na-K}E_{Na-K}$$
$$+ B_{K-F}E_{K-F} + B_{K-K}E_{K-K} + B_{F-F}E_{F-F}$$

Where, E: the internal energy of the molten salt

$B_{Li-F}, B_{Li-Li}, B_{Li-Na}, B_{Li-K}, B_{Na-F}, B_{Na-Na}, B_{Na-K}, B_{K-F}, B_{K-K}, B_{F-F}$: the bonds number of each type.

$E_{Li-F}, E_{Li-Li}, E_{Li-Na}, E_{Li-K}, E_{Na-F}, E_{Na-Na}, E_{Na-K}, E_{K-F}, E_{K-K}, E_{F-F}$: the bonds energy of each type.

$$N_{Li}z_{Li} = 2B_{Li-Li} + B_{Li-F} + B_{Li-Na} + B_{Li-K} \quad (43)$$

$$N_{Na}z_{Na} = 2B_{Na-Na} + B_{Na-F} + B_{Li-Na} + B_{Na-K} \quad (44)$$

$$N_{K}z_{K} = 2B_{K-K} + B_{K-F} + B_{Na-K} + B_{Li-K} \quad (45)$$

$$N_{F}z_{F} = 2B_{F-F} + B_{Na-F} + B_{Li-F} + B_{K-F} \quad (46)$$

Where, $N_{Li}, N_{Na}, N_{K}, N_{F}$: the number of Li, Na, K, F

$z_{Li}, z_{Na}, z_{K}, z_{F}$: the coordination number of each atom in terms of reference atom in the solution

Therefore,

$$B_{Li-Li} = \frac{N_{Li}z_{Li}}{2} - \frac{B_{Li-F} + B_{Li-Na} + B_{Li-K}}{2} \quad (47)$$

$$B_{Na-Na} = \frac{N_{Na}z_{Na}}{2} - \frac{B_{Na-F} + B_{Li-Na} + B_{Na-K}}{2} \quad (48)$$

$$B_{K-K} = \frac{N_{K}z_{K}}{2} - \frac{B_{K-F} + B_{Na-K} + B_{Li-K}}{2} \quad (49)$$

$$B_{F-F} = \frac{N_F z_F}{2} - \frac{B_{Na-F} + B_{Li-F} + B_{K-F}}{2} \tag{50}$$

Substitute the equation *(47)*, *(48)*, *(49)* and *(50)* into *(42)*, then,

$$\begin{aligned} E = {} & \frac{N_{Li} z_{Li} E_{Li-Li}}{2} + \frac{N_{Na} z_{Na} E_{Na-Na}}{2} + \frac{N_K z_K E_{K-K}}{2} \\ & + \frac{N_F z_F E_{F-F}}{2} \\ & + B_{Li-F}\left(E_{Li-F} - \frac{E_{Li-Li} + E_{F-F}}{2}\right) \\ & + B_{Li-F} E_{Li-F} \\ & - E_{Li-Li} \frac{B_{Li-F} + B_{Li-Na} + B_{Li-K}}{2} \\ & + B_{Li-Na} E_{Li-Na} + B_{Li-K} E_{Li-K} \\ & + B_{Na-F} E_{Na-F} \\ & - E_{Na-Na} \frac{B_{Na-F} + B_{Li-Na} + B_{Na-K}}{2} \\ & + B_{Na-K} E_{Na-K} + B_{K-F} E_{K-F} \\ & - E_{K-K} \frac{B_{K-F} + B_{Na-K} + B_{Li-K}}{2} \\ & - E_{F-F} \frac{B_{Na-F} + B_{Li-F} + B_{K-F}}{2} \end{aligned} \tag{51}$$

Since in equation *(51)*,

$$\frac{N_{Li}z_{Li}E_{Li-Li}}{2}+\frac{N_{Na}z_{Na}E_{Na-Na}}{2}+\frac{N_{K}z_{K}E_{K-K}}{2} \quad (52)$$

$$+\frac{N_{F}z_{F}E_{F-F}}{2}$$

$$= energy\ of\ the\ unmixed\ component$$

Then, the heat of formation ΔH_{mix} can be expressed by,

$$\Delta H_{mix} = H_2 - H_1 \quad (53)$$

$$= B_{Li-F}\left(E_{Li-F}-\frac{E_{Li-Li}+E_{F-F}}{2}\right)$$

$$+ B_{Li-F}E_{Li-F}$$

$$- E_{Li-Li}\frac{B_{Li-F}+B_{Li-Na}+B_{Li-K}}{2}$$

$$+ B_{Li-Na}E_{Li-Na}+B_{Li-K}E_{Li-K}$$

$$+ B_{Na-F}E_{Na-F}$$

$$- E_{Na-Na}\frac{B_{Na-F}+B_{Li-Na}+B_{Na-K}}{2}$$

$$+ B_{Na-K}E_{Na-K}+B_{K-F}E_{K-F}$$

$$- E_{K-K}\frac{B_{K-F}+B_{Na-K}+B_{Li-K}}{2}$$

$$- E_{F-F}\frac{B_{Na-F}+B_{Li-F}+B_{K-F}}{2}$$

4.3. Results and Analysis

4.3.1. **Structure Information of FLiNaK**

As shown in Figure 4-1, it is a snapshot of the local ionic structure in the simulation box for FLiNaK. From the statistical calculation of ions' trajectories, the important structure information including the radial distribution function and coordination number distribution were obtained based on the analysis in section 4.2.2. Since structure is extremely sensitive to the simulation model, the structural information of constituent ions of FLiNaK was analyzed and compared with the literature and experimental measurements to validate the FPMD modeling of molten fluoride salts. The radial distribution functions (RDF) of different ion pairs and corresponding coordination numbers in molten FLiNaK salt are shown in Figure 4-2, Figure 4-3, Figure 4-4 and Figure 4-5. The comparison summary between the predicted structure data in this study with the literature [40] and experimental data [50] are also shown in Table 4-1 and Table 4-2. As shown in Table 4-2, the average bond length which correspond to the first peak radius of Li-F, Na-F, K-F and F-F ion pairs were in good agreement with the literature and experiment data. The first shell coordination numbers which were determined by the integral of the RDF in terms of corresponding first peak interval were also compared in Table 4-2. The coordination number predicted in this FPMD agrees well with the literature, but shows greater values than the experiment data. As for the Na-F, K-F and F-F, the lower interval values as pointed by the arrow in Figure 4-3, Figure 4-4 and Figure 4-5 shows a wide flat zone which make the range of the first peak larger thus leading to the large difference between the FPMD and experiment data. But, since our FPMD results match well with the literature FPMD study, it has demonstrated that our method has a good performance in the simulation model.

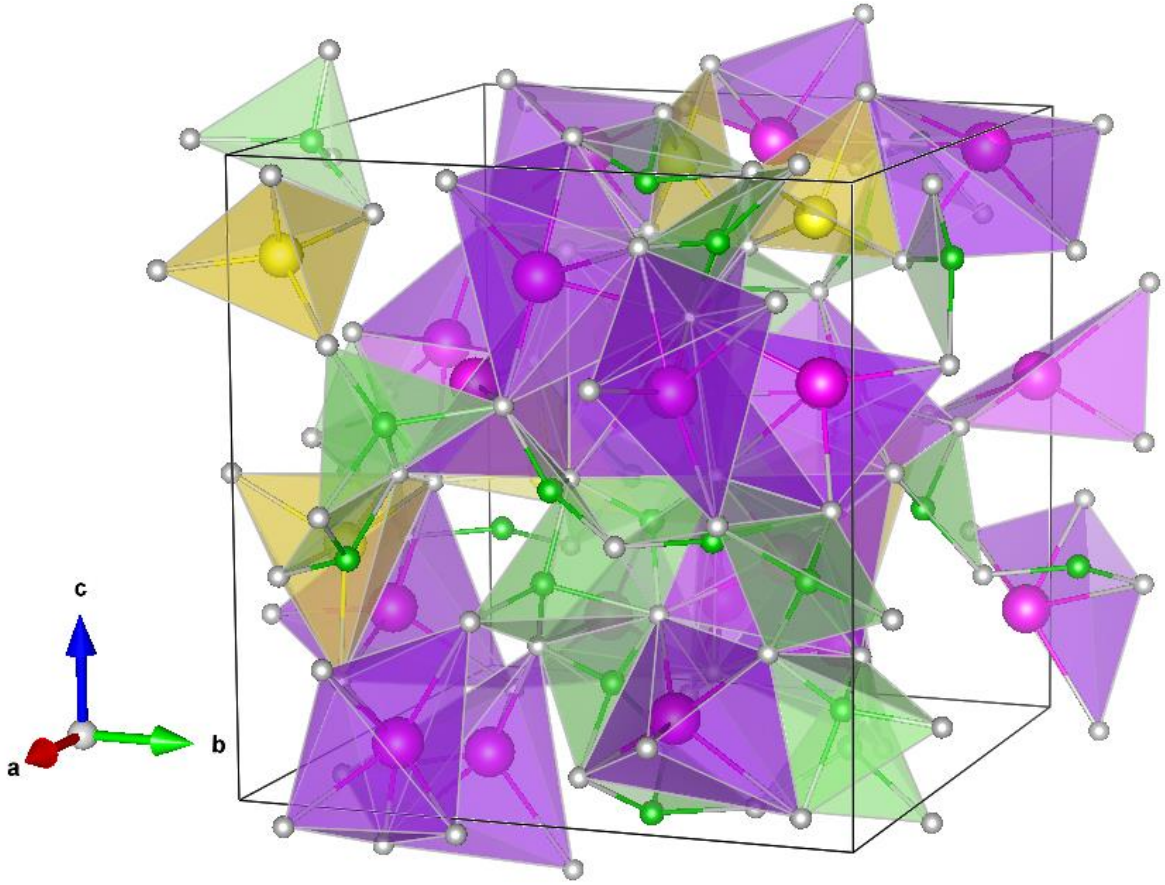

Figure 4-1 Snapshot of the local ionic structure in FLiNaK molten salt at 700°C, grey balls are fluorine ions, green balls are lithium ions, yellow balls are sodium ions, pink balls are potassium balls.

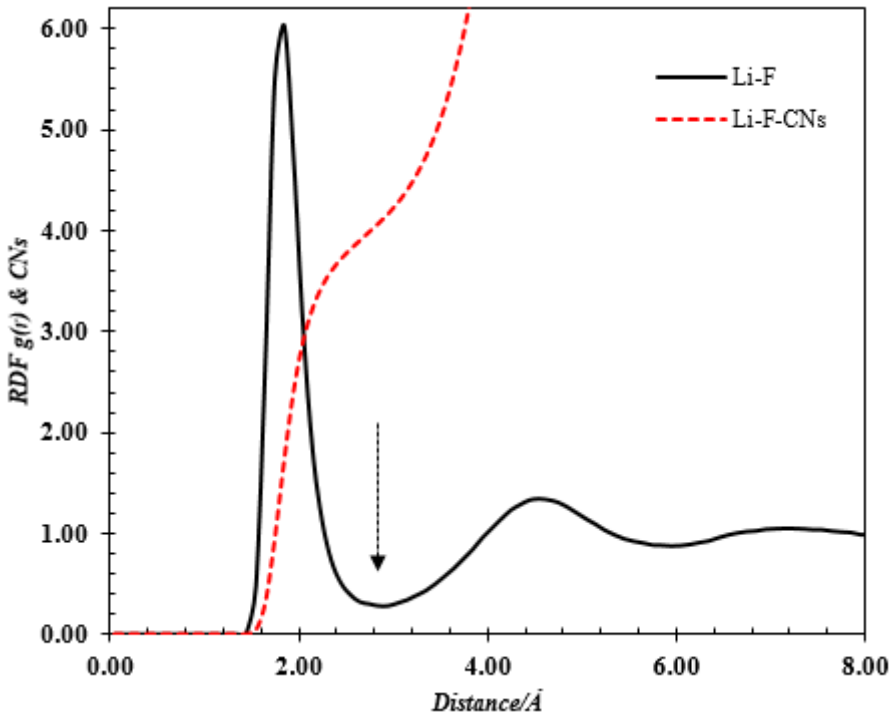

Figure 4-2 Radial distribution function (RDF) of Li-F in FLiNaK at 700°C

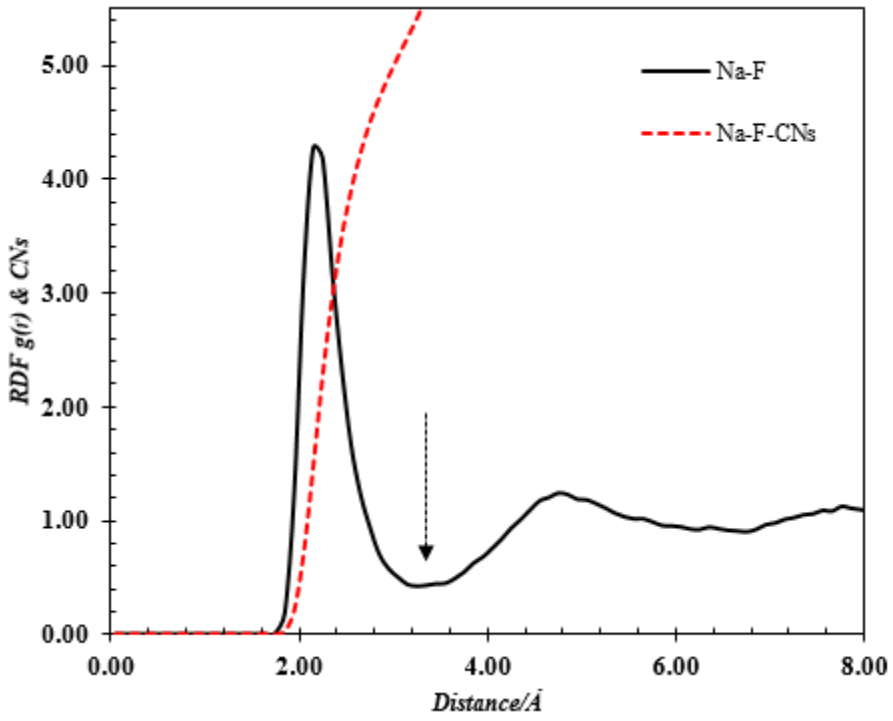

Figure 4-3 Radial distribution function (RDF) of Na-F in FLiNaK at 700°C

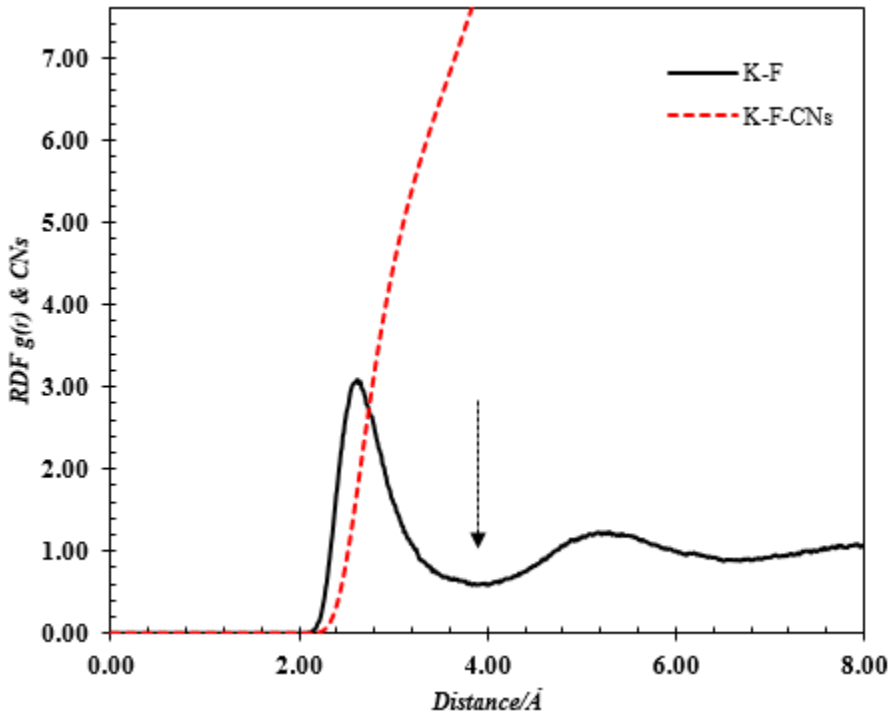

Figure 4-4 Radial distribution function (RDF) of K-F in FLiNaK at 700°C

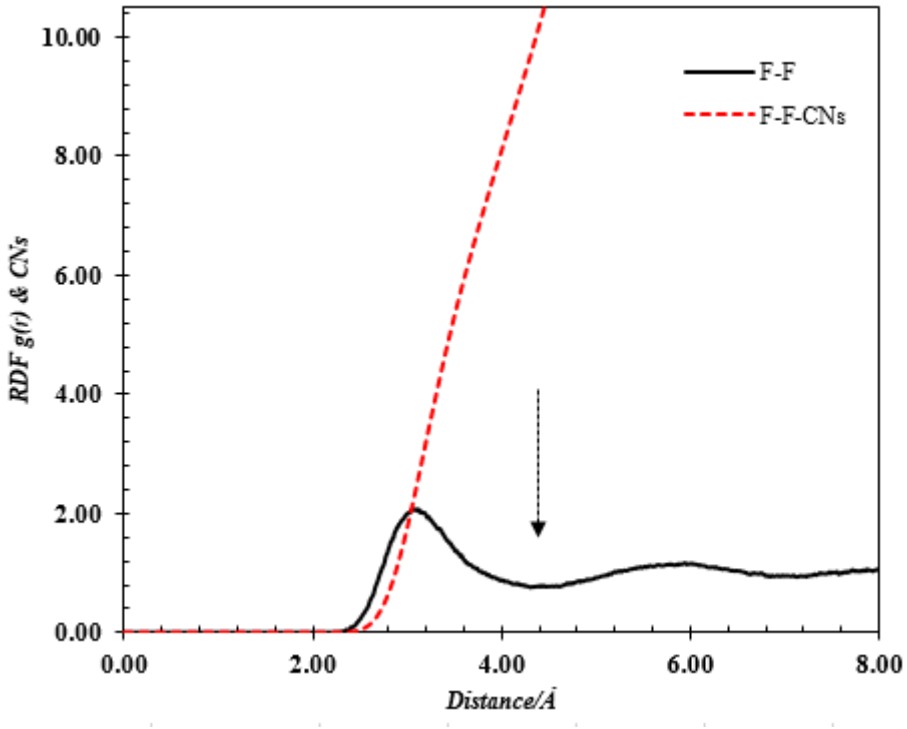

Figure 4-5 Radial distribution function (RDF) of F-F in FLiNaK at 700°C

Table 4-1 Comparison of the first peak radius for ion pairs in FLiNaK with literature data and experiment data. FPMD simulations for FLiNaK were performed at 700°C

	First peak radius Å		
Ion pair	FPMD 700℃	Literature FPMD[41] 700℃	Experiment[50] 520℃
Li^+-F^-	1.85	1.86	1.83
Na^+-F^-	2.17	2.19	2.18
K^+-F^-	2.62	2.59	2.59
F^--F^-	3.07	3.13	3.05

Table 4-2 Comparison of first shell coordination numbers for ion pairs in FLiNaK with literature data and experiment data. FPMD simulations for FLiNaK were performed at 700°C

	Coordination number		
Ion pair	FPMD 700℃	Literature FPMD 700℃	Experiment 520℃
Li^+-F^-	4.0	4.0	3.3
Na^+-F^-	5.4	5.4	3.8
K^+-F^-	7.5	7.3	4.0
F^--F^-	10.3	10.2	8.9

4.3.2. **Structure Information of FLiNaK-La_2O_3**

The local ionic structure of the FLiNaK-La_2O_3 was shown in Figure 4-6. Since there are only two La atoms included in the simulation box. It is observed that on La ion is bonded with five fluorine ions to form a pentahedron structure, while the other one is bonded with both fluorine ions and oxygen ions which should correspond to LaOF as confirmed in section 2.3.

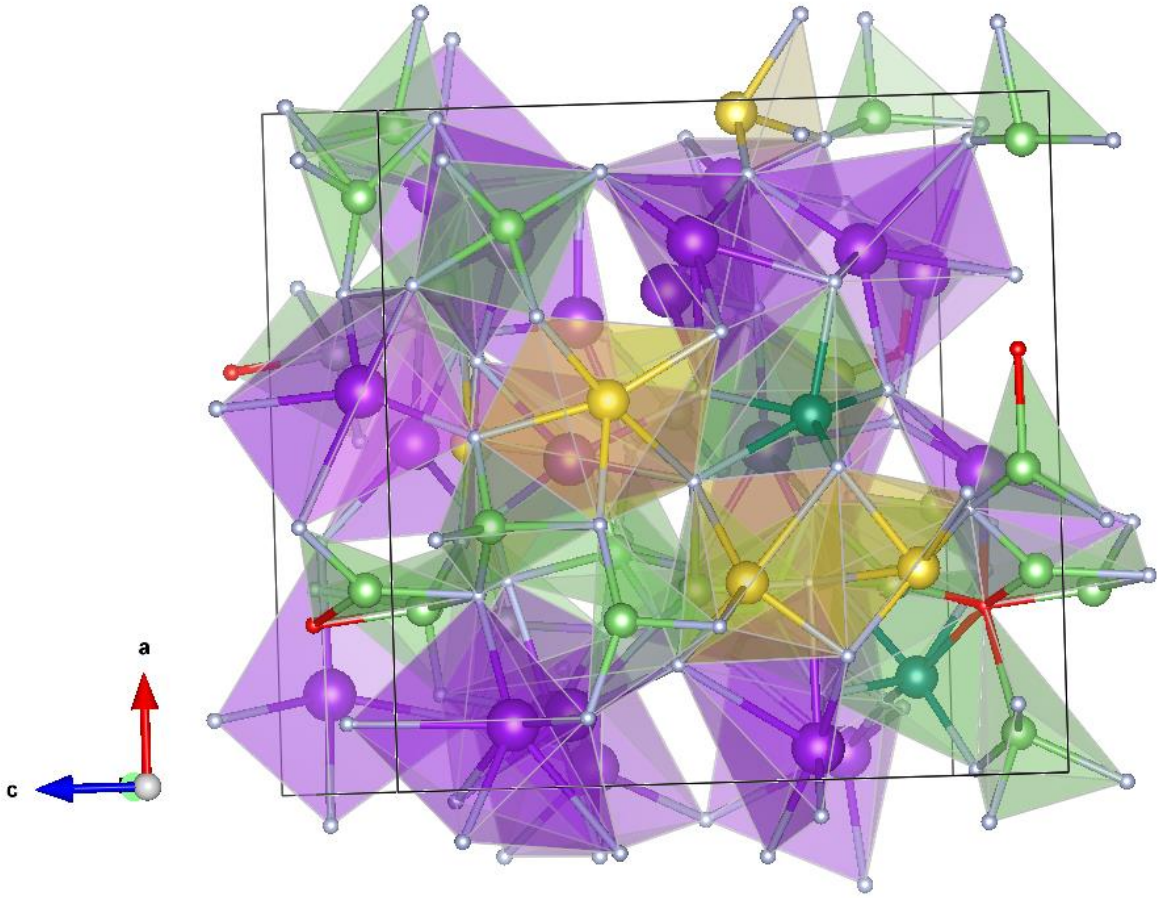

Figure 4-6 Snapshot of the local ionic structure in FLiNaK-La_2O_3 molten salt at 700°C, grey balls are fluorine ions, light green balls are lithium ions, yellow balls are sodium ions, purple balls are potassium ions, deep green balls are lanthanum ions, red balls are oxygen ions.

The first peak radius and first shell coordination number were also calculated in the FLiNaK-La_2O_3 system. The comparison with the data of pure FLiNaK was shown in Table 4-3. There is no significant difference between them in the first peak radius and coordination number for the ionic pairs of Li^+-F^-, Na^+-F^-, but the first peak radius and coordination number of ions pair K^+-F^- and F^--F^- have slight decrease due to the bond related to La^{3+} and F^-.

Table 4-3 Comparison of first peak radius and first shell coordination numbers for ions pairs in FLiNaK and FLiNaK- La_2O_3. FPMD simulations for FLiNaK were performed at 700°C

	FLiNaK-La_2O_3		FLiNaK	
Ion pair	First peak radius Å	Coordination number	First peak radius Å	Coordination number
Li^+-F^-	1.85	4.0	1.85	4.0
Na^+-F^-	2.17	5.4	2.17	5.4
K^+-F^-	2.57	7.4	2.62	7.5
F^--F^-	3.05	9.1	3.07	10.3
La^{3+}-F^-	2.35	7.6	-	-
Li^+-O^{-2}	1.85	0.28	-	-
Na^+-O^{-2}	2.25	0.22	-	-
K^+-O^{-2}	2.65	0.25	-	-
F^--O^{-2}	3.25	0.41	-	-
La^{3+}-O^{-2}	2.15	0.15	-	-

Note: for the corresponding radial distribution function curves, please see the Appendix.

4.3.3. **Enthalpy of Formation ΔH_{mix}**

The total energy from the FPMD simulation with the 100-atom unit cell which includes 23Li, 6Na, 21K and 100F and the 105-atom unit cell which includes 23Li, 6Na, 21K, 100F, 2La and 3O were used to estimate enthalpy of formation (heat of formation) ΔH_{mix} in the molten salt as shown in Table 4-4.

Table 4-4 Comparison of enthalpy of formation in FLiNaK and FLiNaK-La_2O_3

	ΔH_{mix}	Literature
	kJ/mol	kJ/mol
FLiNaK	-583.207 ± 0.840	-
FLiNaK-La_2O_3	-398.397 ± 2.557	-

There is no available literature data to compare with the obtained enthalpy of formation ΔH_{mix} data. But since the validity of simulation method has been confirmed in section 4.3.1, the obtained results should be acceptable. In addition, the Gibbs free energy of LaOF and LaF_3 at 1200℃ were also calculated with quasi-harmonic approximation as shown in Table 4-5. As for LaF_3, the relative error compared with the literature data is 3.67% which indicates good agreement. While for LaOF, there has not been available data to compare.

Table 4-5 Gibbs free energy of LaOF and La_2O_3 at 1200℃

	Gibbs free energy	Literature [51]
	kJ/mol	kJ/mol
LaOF	-2101.916 ± 0.343	-
LaF_3	-2049.677 ± 1.374	-1974.437

4.4. Conclusions and Future work

In this study, structure information of FLiNaK was obtained and compared with the literature and experiment data. The first peak radius agrees well with the literature FPMD and experiment data, while the coordination number can only match well with the literature FPMD, but much larger than the experiment due to the flat zone of the first peak interval which is an issue that also existed in the literature FPMD. Meanwhile, the local ionic structure information of FLiNaK-La_2O_3 was also calculated and the appearance of bond La-O-F matched the data in section 2.3. Meanwhile, it's also possible that the bond of La-O-F has effect on the structure of ion pairs K^+-F^- and F^--F^- in FLiNaK-La_2O_3 system. As for enthalpy of formation in pure FLiNaK and FLiNaK-La_2O_3, total energy from FPMD simulation was used to do the calculation. In addition, Gibbs free energy of LaF_3 and LaOF were obtained based on quasi-harmonic approximation, among which, the data of LaF_3 only has 3.67% relative error compared with literature [51]. Since transport properties, e.g. self-diffusion coefficient, have been not analyzed, more work will be done to further study this field in the future.

Reference

[1] Molten Salt Reactor, https://en.wikipedia.org/wiki/Molten_salt_reactor

[2] LeBlanc, D., "Molten salt reactors: A new beginning for an old idea", Nuclear Engineering and Design, 2010.

[3] D. F. Williams, L. M. Toth, K. T. Clarno, "Assessment of Candidate Molten Salt Coolants for the Advanced High-Temperature Reactor (AHTR)", Oak Ridge National Laboratory, ORNL/TM-2006/12.

[4] Molten Salt Chemistry Workshop, Report for the US Department of Energy, Office of Nuclear Energy Workshop, Oak Ridge National Laboratory, April 10-12, 2017.

[5] Nuclear Separations Technologies Workshop Report, Getting From Where We Are to Where We Want To Be in Nuclear Separations Technologies, Department of Energy, July 27-28, 2011.

[6] T. J. Dolan, Molten Salt Reactor and Thorium Energy, Woodhead Publishing, Jun 8, 2017.

[7] X. L. Guo, J. Sietsma, Y. X. Yang, "Solubility of Rare Earth Oxides in Molten Fluorides", ERES2014: 1st European Rare Earth Resource Conference, 2014.

[8] W. Wu, J. Sun, L. Hai H. Gao, "Nd_2O_3 Solubility in Fluoride Melt", Chin. Rare Earths, 12(3) 34-37 (1991).

[9] M. Ambrová., et al, "On the Solubility of Lanthanum Oxide in Molten Alkali Fluorides" , Journal of Thermal Analysis and Calorimetry, 91(2008): 569-573.

[10] R. M. Wheat., et al, "Solubility of Lanthanum Oxide, Samarium Oxide and Holmium Oxide in the eutectic melt LiF-NaF-KF", Report of the National Academy of Sciences of Ukraine, 4(2011): 132-138.

[11] A. J. Bard, L. R. Faulkner, “Electrochemical Methods: Fundamentals and Applications”, John Wiley & Sons, Inc.

[12] P. Souček, F. Lisý., et al, “Development of electrochemical Separation Methods in Molten LiF-NaF-KF for the Molten Salt Reactor Fuel Cycle”, Journal of Nuclear Science and Technology, 42(2005): 1017-1024.

[13] M. Straka, L. Szatmáry, M. Mareček, J. Uhlír, “On the Posibility of Quantitative Electrochemical Separation of Uranium from Gadolinium in Fluoride Melts”, Transaction of the American Nuclear Society, 118(2018): 118-119.

[14] S. I. Pyun et al., “Electrochemistry of Insertion Materials for Hydrogen and Lithium”, Monographs in Electrochemistry, Springer, 2012.

[15] A. Bard, L. R. Faulkner, Electrochemical Methods: Fundamentals and Applications, John Wiley & Sons, N.Y. 1980.

[16] A. W. Bott, “Controlled Current Techniques”, Current Separations 18(2000): 125 – 127.

[17] E. Stefanidaki, C. Hasiotis, C. Kontoyannis, “Electrodeposition of neodymium from LiF-NdF_3-Nd_2O_3”, Electrochinica Acta, 46(2001): 2665-2670.

[18] S. I. Berul, N. K. Voskresenskaya, Zh. Neorg. Khim, 8(1963): 1431.

[19] Z.X. Qiu, M.J. Zhang, “Studies on Anode Effect in Molten-Salts Electrolysis”, Electrochim Acta, 32(1987): 607–613.

[20] Lifang T, Wei Huang, Feng Jiang., et al, “Electrochemical Behavior of Graphite Anode in LiF-NaF-KF Eutectic with YF3”, Electrochimica Acta, 225(2017): 392-398.

[21] M. Ambrova, J. Jurisova, A. Sykorova., et al, “Electrochemical behavior of the LiF-CaF_2-La_2O_3 system”, Chemical Papers, 62(2008): 154-159.

[22] Huan Qiao, T. Nohira, Y. Ito, “Electrochemical Behavior of Oxide Ion at a Glassy Carbon Electrode in a LiF-NaF-KF Eutectic Melt”, 71(2003): 530-535.

[23] Zuoju Huang, Zhanmin Cao, Guihua Wang, Hongmin Zhu, “An Electrochemical Study of Electrode Process on Carbon Electrode in LiF-NaF-KF Melt”, Electrochemistry, 78(2010): 510-512.

[24] Shaoqiang Guo, N. Shay, Y. Wang, W. Zhou, J. Zhang, “Measurement of Europium(III)/Europium(II) Couple in Fluoride Molten Salt for Redox Control in a Molten Salt Reactor Concept”, Journal of Nuclear Materials, 496(2017): 197-206.

[25] T. Yamamura, M. Mehmood, H. Maekawa, Y. Sato, “Electrochemical Processing of Rare-Earth and Rare Metal by Using Molten Salts”, Chemistry for Sustainable Development, 12(2004): 105-111.

[26] Devin Rappleye and Michael F. Simpson, "Electrochemical Signal Measurement and Analysis for Metal Deposition in Molten LiCl-KCl Eutectic," in INMM 56th Annual Meeting, Palm Springs, CA, July 2015.

[27] Y. Ito, T. Takenaka, K. Ema, J. Oishi, Electrochemistry, 51(1983):864.

[28] G. Chen, Z. N. Shi, et al, “Anodic Passivation of a Graphite Electrode in LiF-KF Melt at 773K”, Journal of The Electrochemical Society, 162(2015): C197-C204.

[29] W. Kohn, L. J. Sham, “Self-Consistent Equations Including Exchange and Correlation Effects”, Physical Review Journals Archive, 140(1965): A1133-A1138.

[30] R. Car, M. Parrinello, “Unified Approach for Molecular Dynamics and Density Functional Theory”, Physical Review Letters, 55(1985): 2471-2474.

[31] G. Kresse, J. Hafner, “Ab Initio Molecular Dynamics for Liquid Metals”, Physical Review B, 47(1993): 558-561.

[32] G. Kresse, J. Furthmüller, “Efficiency of Ab-initio Total Energy Calculations for Metals and Semiconductors Using a Plan-wave Basis Set”, Computational Materials Science 6 (1996) 15–50.

[33] CPMD, http://www.cpmd.org/, jointed copyright by IBM Corporation and Max-Planck Institut, Stuttgart.

[34] G. Kresse, D. Joubert, “From Ultrasoft Pseudopotentials to the Projector Augmented-Wave Method”, Physical Review B, 59(1999): 1758-1775.

[35] G. Kresse, J. Furthmuller, “Efficient Iterative Schemes for Ab Initio Total Energy Calculations Using a Plan-wave Basis Set”, Physical Review B, 54(1996): 169-186.

[36] D. Alfe, M. J. Gillan, “First-Principles Calculation of Transport Coefficients”, Physical Review Letters, 81(1998): 5161-5164.

[37] H.Z. Fang, W.Y. Wang, P.D. Jablonski, Z.K. Liu, “Effects of Reactive Elements on the Structure and Diffusivity of Liquid Chromia”, Physical Review B, 85(2012): (014207)1-(014207)10.

[38] P. Ganesh, M. Widom, “Liquid-Liquid Transition in Supercooled Silicon Determined by First-Principles Simulation”, Physical Review Letters, 102(2009): (075701)1-(075701)4.

[39] A. Bengtson, H.O. Nam, S. Saha, R. Sakidja, D. Morgan, “First-principles Molecular Dynamics Modeling of the LiCl-KCl Molten Salt System”, Computational Materials Science, 83(2014): 362-370.

[40] H.O. Nam, A. Bengtson, K. Vortler, S. Saha, R. Sakidja, D. Morgan, “First-principles Molecular Dynamics Modeling of the Molten Fluoride Salt with Cr Solute”, Journal of Nuclear Materials, 449(2014): 148-157.

[41] J. Dai, H. Han, Q. Li, P. Huai, “First-principle Investigation of the Structure and Vibrational Spectra of the Local Structures in LiF-BeF_2 Molten Salt”, Journal of Molecular Liquids, 213(2016): 17-22.

[42] J. Song, S. Shi, X. Li, L. Yan, “First Principle Molecular Dynamics Modeling of UCl_3 in LiCl-KCl Eutectic”, Journal of Molecular Liquids, 234(2017): 279-286.

[43] S. Nosé, “A Unified Formulation of the Constant Temperature Molecular Dynamcis Methods”, J. Chem. Phys. 81 (1984) 511–519.

[44] X. Lv, Z. Han, J. Chen, L. Jiang, Z. Xu, Q. Liu, “First-principles Molecular Dynamics Studies of Ionic Structure and Transport Properties of LiF-NaF-AlF_3 Molten Salt”, Chemistry Physics Letters, 706(2018): 237-242.

[45] X. Lv, Z. Xu, J. Li, J. Chen, Q. Liu, “First-principles Molecular Dynamics Investigation on Na3AlF6 Molten Salt”, Journal of Fluorine Chemistry, 185(2016): 42-47.

[46] L. Martínez, R. Andrade, E.G. Birgin, J.M. Martínez, “Packmol: A Package for Building Initial Configurations for Molecular Dynamcis Simulatins” J. Comput. Chem. 30 (2009): 2157–2164.

[47] Shuichi Nose, “A Unified Formulation of the Constant Temperature Molecular Dynamics Methods”, J. Chem. Phys. 81(1984): 511-519.

[48] W.H. Press, B.P. Flannery, S.A. Teukolsky and W.T. Vetterling, “Numerical Recipes: The Art of Scientific Computing (Third Edition)”, Cambridge University Press, New York, 1986.

[49] J.M. Ziman, Principles of the Theory of Solids Cambridge, Cambridge University Press, Cambridge University, 1972.

[50] K. Igarashi, Y. Okamoto, J. Mochinaga, H. Ohno, “X-Ray Diffraction Study of Molten Eutectic LiF-NaF-KF Mixture”, J. Chem. Soc., Faraday Trans. 1: Phys. Chem. Condens. Phases, 84(1988): 4407–4415.

[51] HCP Chemistry 6, Barin 95.

Appendix A

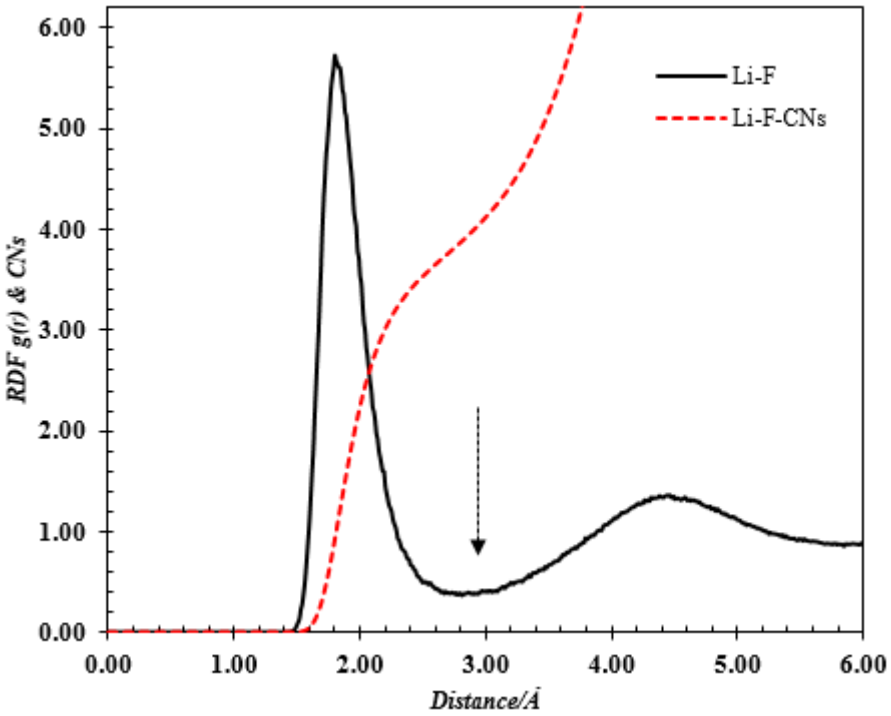

Figure A-1 Radial distribution function (RDF) of Li-F in FLiNaK-La_2O_3 at 700°C

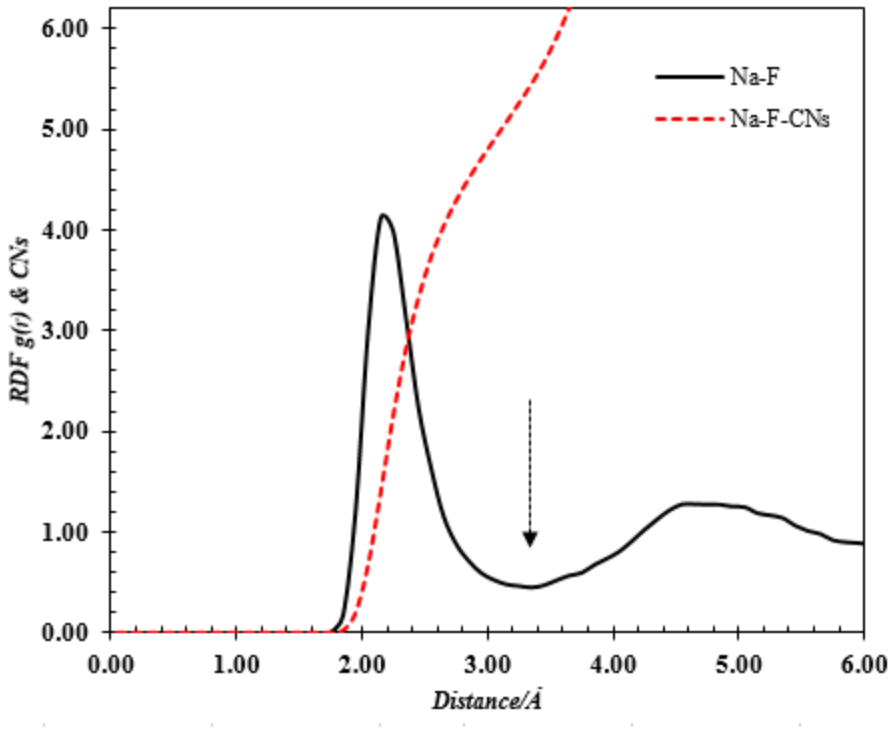

Figure A-2 Radial distribution function (RDF) of Na-F in FLiNaK-La_2O_3 at 700°C

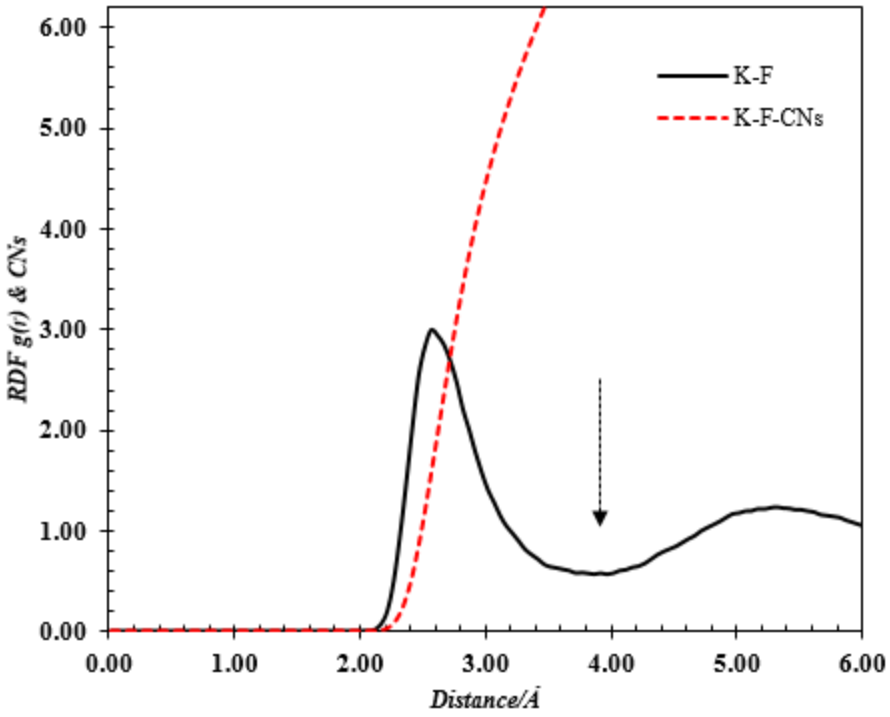

Figure A-3 Radial distribution function (RDF) of K-F in FLiNaK-La_2O_3 at 700°C

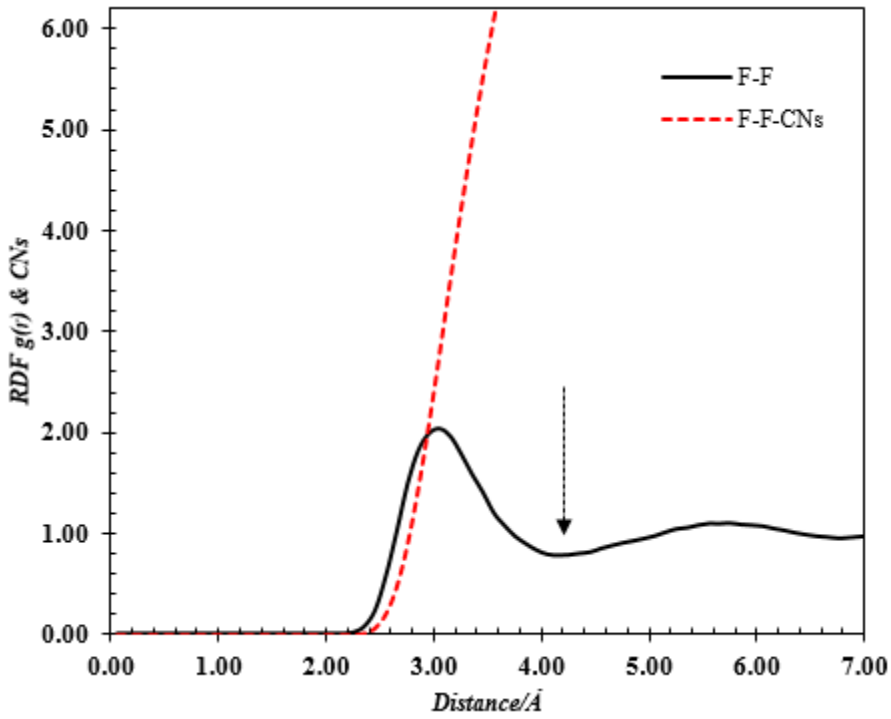

Figure A-4 Radial distribution function (RDF) of F-F in FLiNaK-La_2O_3 at 700°C

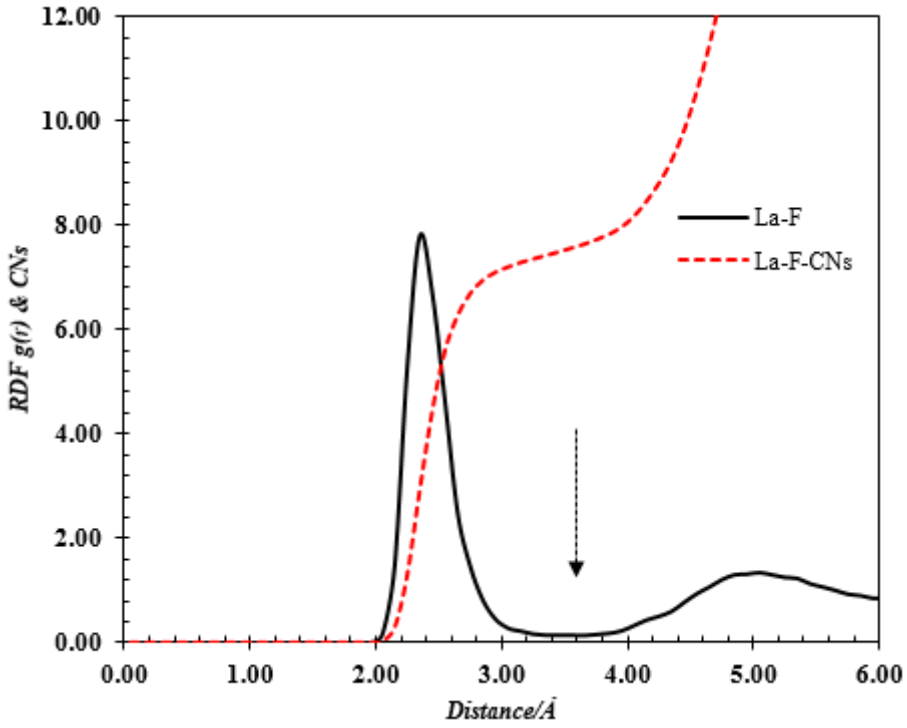

Figure A-5 Radial distribution function (RDF) of La-F in FLiNaK-La_2O_3 at 700°C

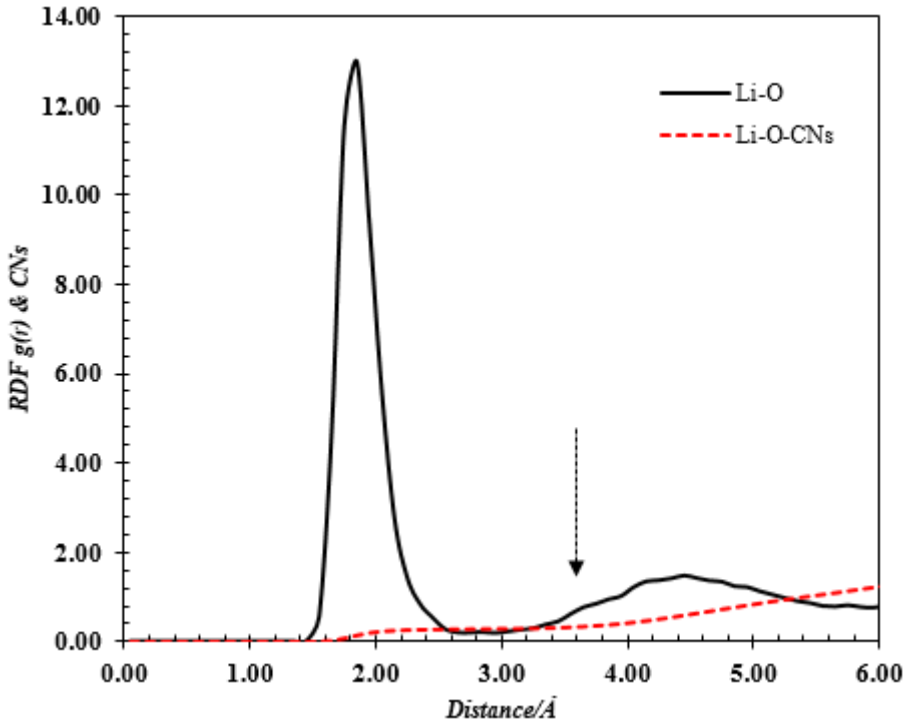

Figure A-6 Radial distribution function (RDF) of Li-O in FLiNaK-La_2O_3 at 700°C

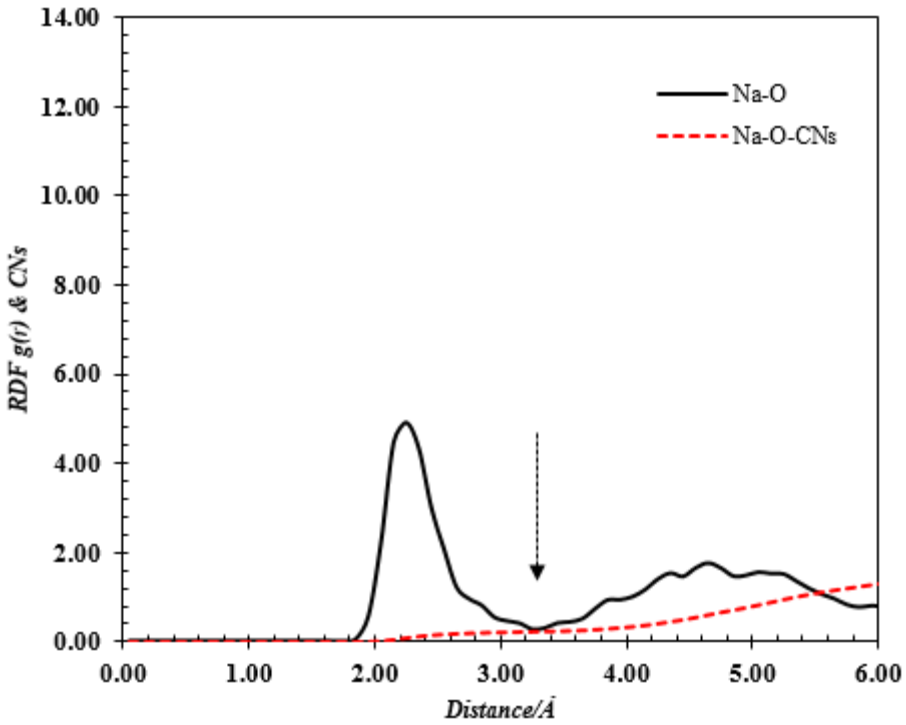

Figure A-7 Radial distribution function (RDF) of Na-O in FLiNaK-La_2O_3 at 700°C

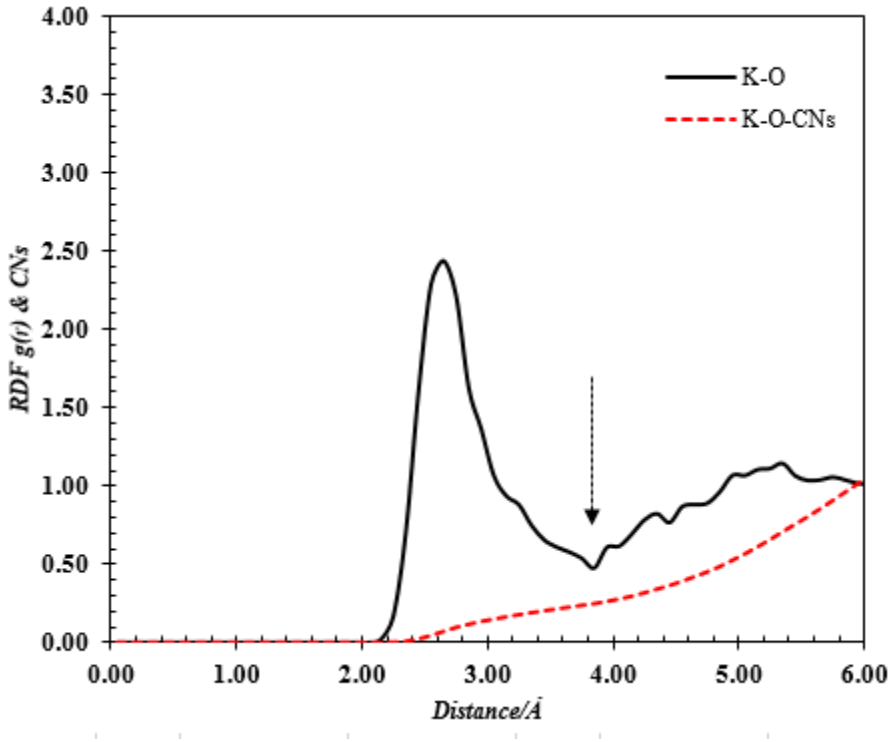

Figure A-8 Radial distribution function (RDF) of K-O in FLiNaK-La_2O_3 at 700°C

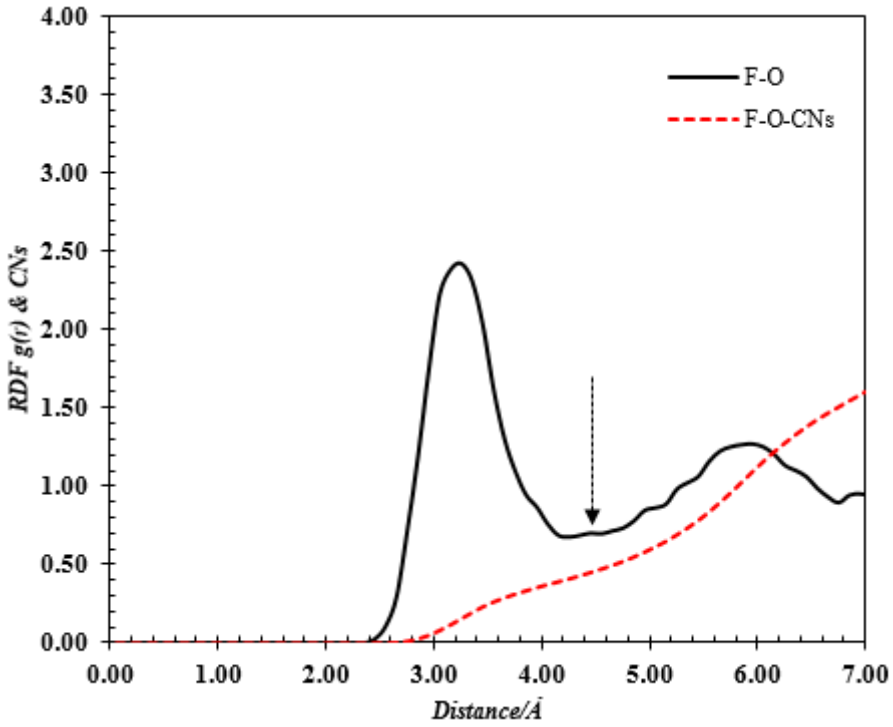

Figure A-9 Radial distribution function (RDF) of F-O in FLiNaK-La_2O_3 at 700°C

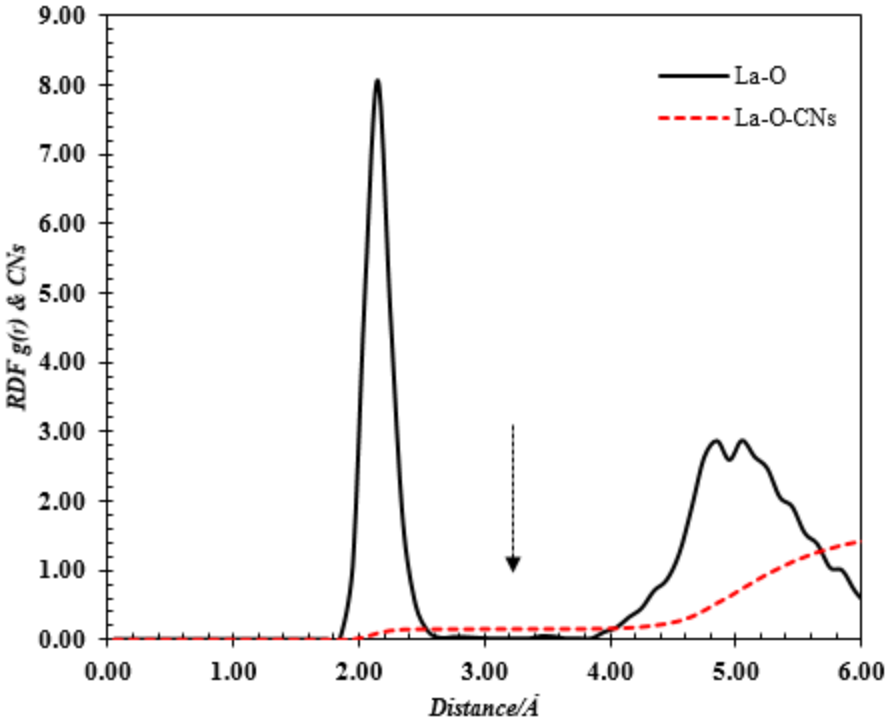

Figure A-10 Radial distribution function (RDF) of La-O in FLiNaK-La_2O_3 at 700°C